T-3848

LOW TEMPERATURE SOLID STATE BONDING OF COPPER USING SPUTTERED SILVER INTERLAYERS

by

Alan M. Meier

ARTHUR LAKES LIBRARY
COLORADO SCHOOL of MINES
GOLDEN, COLORADO 80401

ProQuest Number: 10783576

All rights reserved

INFORMATION TO ALL USERS
The quality of this reproduction is dependent upon the quality of the copy submitted.

In the unlikely event that the author did not send a complete manuscript
and there are missing pages, these will be noted. Also, if material had to be removed,
a note will indicate the deletion.

ProQuest 10783576

Published by ProQuest LLC (2018). Copyright of the Dissertation is held by the Author.

All rights reserved.
This work is protected against unauthorized copying under Title 17, United States Code
Microform Edition © ProQuest LLC.

ProQuest LLC.
789 East Eisenhower Parkway
P.O. Box 1346
Ann Arbor, MI 48106 – 1346

T-3848

A thesis submitted to the Faculty and the Board of Trustees of the Colorado School of Mines in partial fulfillment of the requirements for the degree of Master of Science (Materials Science).

Golden, Colorado

Date April 6, 1990

Signed: 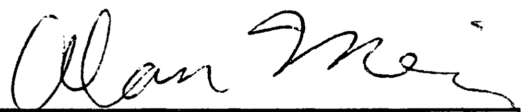

Alan M. Meier

Approved:

Dr. Glen R. Edwards
Thesis Advisor

Golden, Colorado

Date April 6, 1990

Dr. John J. Moore
Professor and Head,
Dept. of Metallurgical & Matls Eng.

ABSTRACT

Magnetron sputter coating was used to apply silver interlayers for solid state bonding. Coating thickness and sputter deposition current were varied and the effects of coating thickness and microstructure on bond strength were examined. Sputter coating was shown to be a viable means of applying coatings for solid state bonding. When copper was bonded using silver interlayers, bond strengths of up to 250 MPa were achieved with a bonding pressure of 65 MPa at 300 °C for 1800 seconds (30 minutes). The most important factor in determining bond strength was the joint thickness. For a joint thickness of 2 μm to 35 μm, surface roughness effects led to a wide range of measured bond strengths and a lowering of the bond strength even though the nominal surface roughness was only 0.25 ± 0.13 μm. From 35 μm to 70 μm, consistently strong bonds (230 to 250 MPa) were produced under all coating conditions due to the development of a triaxial stress state. Several of these bonds even failed in a copper tensile half. From 70 to 86 μm, there was a decrease in strength due to a loss of triaxiality with increasing thickness. Both {111} and {220} preferred orientations were obtained. In the deposition current range of 0.20 to 0.55 amperes, it was possible to predict which orientation would be present for a given coating thickness. For the 6-μm-thick coatings, the bond strength increased with increasing degree of {220} preferred orientation. For the thicker coatings, the bond strength was

independent of orientation. Several different single modal, bimodal and trimodal growth modes were observed in the coating surface morphologies. The different growth modes did not affect the bond strength or the preferred orientation.

TABLE OF CONTENTS

Page

ABSTRACT. iii

LIST OF FIGURES. vii

LIST OF TABLES. xi

ACKNOWLEDGEMENTS. xii

I. INTRODUCTION. 1

A. Background. 1
B. Interlayers. 3
C. Use of Silver Interlayers. 6
D. Sputter Coating. 12

II. EXPERIMENTAL PROCEDURE. 17

A. Sample Machining. 17
B. Coating Procedure. 21
C. Bonding Procedure. 24
D. Mechanical Testing. 27
E. Thickness Measurements. 28
F. Microstructural Examination. 28
G. Test Matrix. 29

III. RESULTS AND DISCUSSION. 32

A. Bond Strength Measurements. 32

A.1. Effect of Thickness on Bond Strength. 33
A.2. Effect of Sputter Deposition Current on Bond Strength 40
A.3. Discussion of Current and Thickness Effects. 43
A.4. Effect of Bonding Pressure and Temperature 45

B. Crystallographic Orientation of Sputtered Coatings 47

B.1. Crystallographic Orientation of As-machined Copper Surfaces. 47
B.2. Effect of Thickness on Orientation. 48

B.3. Effect of Sputter Current on Orientation 52
B.4. Effect of Preferred Orientation on Bond Strength. . 56
B.5. Discussion of Preferred Orientation Effects. 60

C. Microstructure. 63

C.1. As-machined Copper Surfaces. 63
C.2. Coating Morphology. 65
C.3. Discussion of Coating Morphology Effects. 74

D. Fracture Surface Examination. 76

IV. CONCLUSIONS. 82

V. REFERENCES CITED. 85

LIST OF FIGURES

Figure Page

1.1: Upper and lower bounds on joint strength as a function of thickness for an 0.8 mm (0.315 in.) diameter silver butt joint as predicted by Orowan's analysis. 5

1.2: Copper-silver binary phase diagram. 7

1.3: Zone diagram for sputter deposition. Film morphology is shown as a function of homologous temperature and sputtering pressure. 14

2.1: Schematic of bonding coupons showing the sample dimensions prior to bonding and prior to tensile testing. 20

2.2: Cross-section of an as-machined copper surface with an average roughness of 1.1 μm (43 μin). .21

2.3: Schematic of inverted magnetron sputter coating unit. 23

2.4: Schematic of bonding unit. 26

3.1: Bond strength as a function of joint thickness for a sputter deposition current of 0.20 amps. 34

3.2: Bond strength as a function of joint thickness for a sputter deposition current of 0.40 amps. 35

3.3: Bond strength as a function of joint thickness for a sputter deposition current of 0.55 amps. 37

3.4: Bond strength as a function of joint thickness for a sputter deposition current of 0.40 amps and an extended thickness range. 38

3.5: Bond strength versus sputter deposition current for a joint thickness of 12 ± 2 μm. 41

3.6: Bond strength versus sputter deposition current for a joint thickness of 26 ± 4 μm. 42

3.7: Bond strength versus sputter deposition current for a joint thickness of 41 ± 6 μm. 44

3.8: Bond strength as a function of bonding pressure for several temperatures. 46

3.9: Combined plot of preferred orientation versus thickness for .20, .40 and .55 amp sputter deposition currents. 49

3.10: Preferred orientation versus thickness for a .40 amp sputter deposition current over the extended thickness range of 1 μm to 43 μm. 51

3.11: Preferred orientation versus sputter deposition current for a coating thickness of 6 ± 1 μm. 53

3.12: Preferred orientation versus sputter deposition current for a coating thickness of 13 ± 2 μm. 54

3.13: Preferred orientation versus sputter deposition current for a coating thickness of 20 ± 3 μm. 55

3.14: Average bond strength versus degree of preferred orientation for a joint thickness of 12 ± 2 μm. 57

3.15: Average bond strength versus degree of preferred orientation for a joint thickness of 26 ± 4 μm. 58

3.16: Average bond strength versus degree of preferred orientation for a joint thickness of 41 ± 6 μm. 59

3.17: SEM photographs of as-machined copper substrate a.) 200X b.) 2000X. 64

3.18: SEM photograph of as-machined copper substrate showing microtearing (2000X). 64

3.19: Low magnification (200X) SEM photographs of as-coated sample surfaces showing roughened surface and machining lines: a.) 1 μm, 0.40 amps b.) 13 μm, 0.40 amps c.) 13 μm, 0.20 amps d.) 20 μm, 0.40 amps e.) 20 μm, 0.45 amps f.) 43 μm, 0.40 amps. 66

3.20: SEM photographs of surfaces of as-coated 6 ± 1 μm thick sputtered silver coatings (5000X). The samples are arranged from the lowest bond strength to the highest bond strength (from the strongest {111} orientation to the strongest {220} orientation): a.) 0.10 amps b.) 0.70 amps (1st coating run) c.) 0.55 amps d.) 0.40 amps e.) 0.70 amps (2nd coating run) f.) 00.20 amps 68

3.21: SEM photographs of surfaces of as-coated 13 ± 2 μm thick sputtered silver coatings (5000X). The samples are arranged from the strongest {111} orientation to the strongest {220} orientation : a.) 0.55 amps b.) 0.20 amps c.) 0.40 amps (1st coating run) d.) 0.40 amps (2nd coating run) e.) 0.10 amps . .70

3.22: SEM photographs of surfaces of as-coated 20 ± 3 μm thick sputtered silver coatings (5000X). The samples are arranged from the strongest {111} orientation to the strongest {220} orientation : a.) 0.45 amps b.) 0.55 amps c.) 0.50 amps d.) 0.30 amps e.) 0.20 amps f.) 0.40 amps (1st coating run) g.) 0.40 amps (2nd coating run) h.) 0.35 amps 72

3.23: SEM photographs of the 0.40-amp coatings (2000X): a.) 1 μm b.) 2 μm c.) 6 μm d.) 13 μm e.) 20 μm f.) 35 μm g.) 43 μm 73

3.24: Low magnification (25X) photographs of fracture surfaces for several coating thicknesses: a.) 1 μm b.) 2 μm c.) 6 μm d.) 13 μm e.) 20 μm f.) 43 μm. 77

3.25: SEM photographs of fracture surfaces for thin coatings (250X): a.) 1 μm, bond strength = 8 MPa b.) 1 μm, bond strength = 129 MPa c.) 2 μm, bond strength = 179 MPa d.) 2 μm, bond strength = 226 MPa 78

3.26: SEM photographs of fracture surfaces for 20-μm-thick coatings (250X): a.) bond strength = 233 MPa b.) bond strength = 243 MPa c.) bond strength = 243 MPa 80

3.27: SEM photograph of the fracture surface of a 43-μm-thick coating (250X). The bond strength was 118 MPa 81

LIST OF TABLES

Table — Page

1.1: Free energy of formation and equilibrium partial pressure of oxygen at several temperatures for silver and copper oxides. 8

1.2: Relative hardness of several metals and their oxides. 9

2.1: Mechanical properties and chemical composition of electrolytic tough pitch copper (ETP 110). .18

2.2: Coating Parameters. 24

2.3: Bonding Parameters. 27

2.4: Test matrix for constant current sputtered silver coatings showing the number of bonds for a given coating run. 30

2.5: Test matrix for constant thickness sputtered silver coatings showing the number of bonds for a given coating run. 30

3.1: Relative X-ray peak intensities for as-machined copper surfaces. 48

3.2: Schmid factors for slip systems in a silver single crystal with (111) and (220) planes oriented perpendicular to an applied uniaxial stress 62

ACKNOWLEDGMENTS

I would like to acknowledge the Office of Naval Research and the Center for Welding and Joining Research at the Colorado School of Mines for funding this project (ONR Contract # N0014-85K-0504).

I would like to thank my advisor, Dr. Glen Edwards, for his input and for reading through several rough drafts of this work.

I would also like to thank the technical staff at the School of Mines metallurgy department; Bob McGrew, Steve Donnelson and Herb Bird for their assistance. I especially thank Herb Bird without whose help I would not have been able to keep the bonding and coating equipment operating.

Finally, I would like to acknowledge Roger Nichting and Norman Nicholas who worked on this project before me. They were responsible for building all of the experimental equipment and their experimental work made mine possible.

I. Introduction

Silver is frequently used as an interlayer material in solid state bonding because it is relatively ductile and it has a thermally unstable oxide. Bonding is usually done with foils, electrodeposited coatings or vapor deposited coatings. Sputter deposited coatings may lead to stronger bonds because of the improved adhesion between the coating and the substrate. Previous work with other coating techniques has shown that bond strengths can be influenced by both the interlayer thickness and the coating morphology. In this work four areas related to bonding with sputtered silver interlayers were examined:

1. Sputter deposition was evaluated as a means of applying coatings for interlayer bonding.
2. Bond strength was evaluated as a function of coating thickness and sputter deposition current.
3. The coating morphology was characterized as a function of coating thickness and sputter deposition current.
4. An attempt was made to correlate the bond strength with the coating microstructure.

A. Background

Solid-state diffusion bonding is a joining process where two flat surfaces are joined at an elevated temperature using an applied pressure. It is preferred over brazing and conventional welding when sample distortion needs to be minimized, when high temperature phase tranformations are to be avoided and when material incompatibility is a problem. It is an expensive technique due to a

high cost for capital equipment and relatively long bonding times. This limits its use to specialized applications where cost is not a major factor. Some materials in this category which have been successfully bonded include: titanium alloys, nickel-base alloys, berylium alloys, refractory metals; and dissimilar metal combinations such as titanium-stainless steel, titanium-boron, aluminum-stainless steel, aluminum-uranium and stainless steel-uranium [1].

Possible mechanisms for solid-state bonding have been proposed by Derby and Wallach [2,3], and Mohamed and Washburn [4]. The mechanisms consist of two basic steps. The first step is the plastic deformation of surface asperities. In this step initial contact is made and voids are created. The second step is the closure of these voids. This is accomplished either through creep, bulk diffusion, grain boundary diffusion, surface diffusion or a combination of these processes.

The actual metal to metal bonding is not clearly understood. Several possible mechanisms are reviewed by Kazakov [5]. The film hypothesis states that all metals and alloys possess an equal property to seize when clean surfaces are brought together within the range of interatomic forces. In the energy hypothesis, no bonding occurs until the atoms of the metals being joined attain the energy threshold of seizure or adhesion. In the dislocation hypothesis, the joint plastic deformation causes dislocations to move to the surface. As they move to the surface, they break up the oxide films present and produce

steps, each an interatomic distance high. Finally, other mechanisms place an emphasis on recrystallization, formation of a more stable electron configuration or interdiffusion of the bulk specimens.

B. Interlayers

Solid-state bonding can be done directly between two samples or an interlayer can be used. Cline [6] gives five reasons for using interlayers:

1. To promote plastic flow.
2. To provide clean surfaces.
3. To promote diffusion.
4. To provide a diffusion barrier to minimize undesirable intermetallic formation.
5. To temporarily establish eutectic melting to promote diffusion of base metals.

Most diffusion bonding is done in the temperature range of 0.5 to 0.8 T_m. Even at these temperatures, unwanted phase transformations frequently occur. By promoting diffusion and plastic flow, interlayers can be used to lower bonding temperatures (below 0.5 T_m) so that many of these transformations can be avoided.

The use of a soft interlayer material does not necessarily lead to a lowering of the bond strength. Joint tensile strengths in the range of the ultimate tensile strength of the base metal can be achieved due to the development of a triaxial stress state at the joint. The stress distribution of a cylindrical butt joint was first analyzed by Orowan and is reviewed by Saxton, West and Barrett [7]. If the yield stress of the

interlayer is less than that of the base metal, the interlayer will began to deform plastically while the base metal is still elastic. This leads to a transverse contraction of the joint. However, the joint material is constrained by the base material which is not yielding so that transverse stresses increase in the joint. This constraint produces a triaxial stress state which minimizes the shear stress within the joint and prevents appreciable plastic deformation. From calculations involving the stress distribution at the joint, upper and lower limits on the joint strengths were predicted:

$$\sigma_{\substack{\text{upper}\\\text{limit}}} = \sigma_{UTS\ (Ag)} \left(1 + \frac{d}{6t}\right)$$

$$\sigma_{\substack{\text{lower}\\\text{limit}}} = \sigma_{YS\ (Ag)} \left(1 + \frac{d}{6t}\right)$$

where : $\sigma_{UTS\ (Ag)}$ = UTS of bulk silver in uniaxial tension

$\sigma_{YS\ (Ag)}$ = YS of bulk silver in uniaxial tension

d = sample diameter

t = interlayer thickness

In this analysis, the joint strength is a function of the thickness to diameter ratio, not just the thickness. Figure 1.1 shows the upper and lower joint strength limits for silver (YS= 55 MPa and UTS= 125-130 MPa) as a function of thickness with a joint diameter of 8 mm (0.315 in). With a electroytic tough pitch (ETP 110) copper base material,

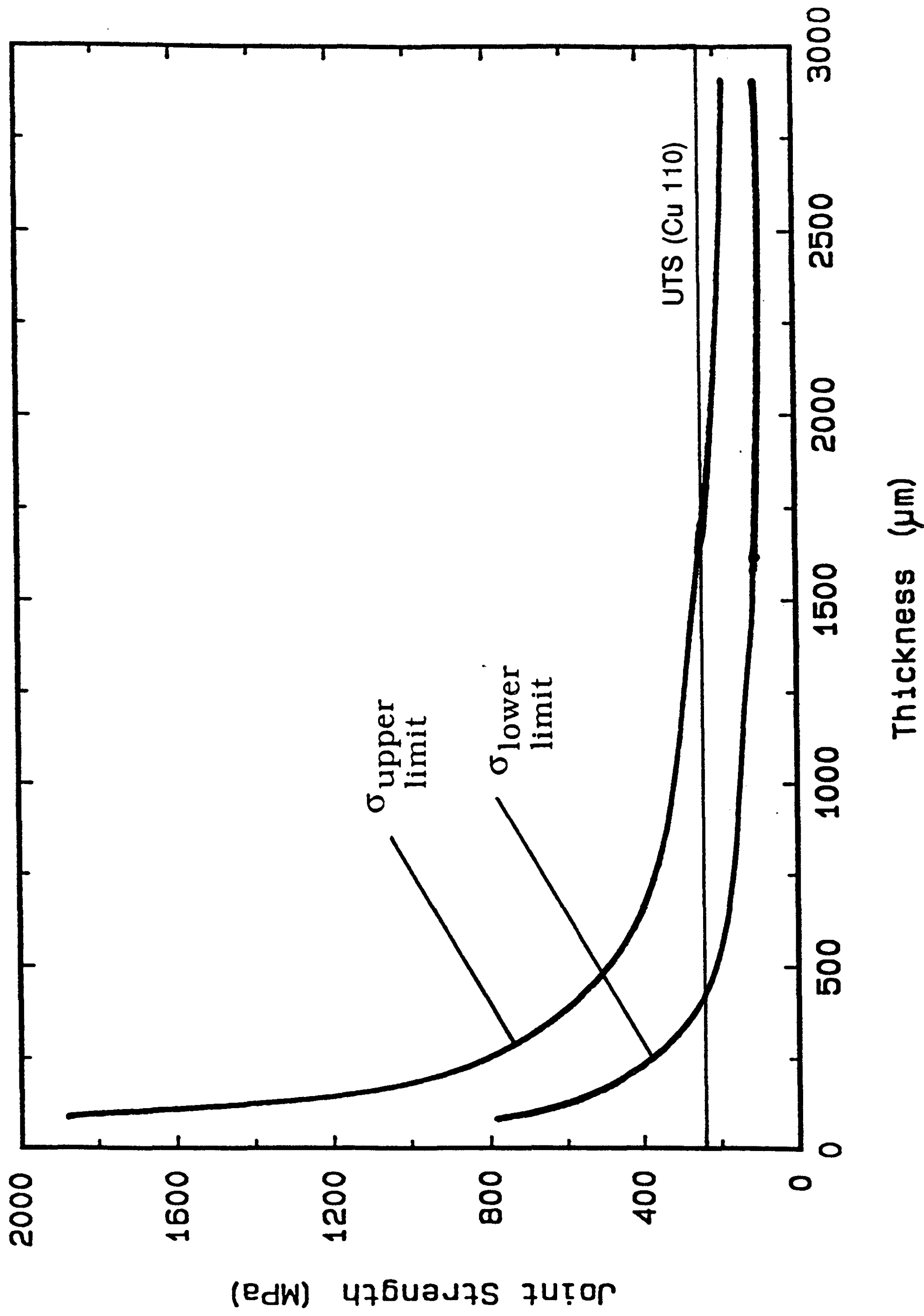

Figure 1.1: Upper and lower bounds on joint strength as a function of thickness for an 8.0 mm (0.315 in.) diameter silver butt joint as predicted by Orowan's analysis.

this model predicts that all joints thinner than 375 μm will fail at the ultimate tensile strength of the ETP 110 copper (240-260 MPa). Two major assumptions are made in the previous analysis:

1. The base material cylinders are assumed to be perfectly rigid.
2. The joint is assumed to be a uniform disc of constant thickness.

The validity of these assumptions will be discussed in the Results and Discussion section of this paper.

C. Use of Silver Interlayers

In this study, a model system was desired so that the effect of interlayer microstructure could be studied without phase transformations complicating the analaysis. The copper-silver system was chosen for several reasons. First, there are no intermetallics in the copper-silver system. The phase diagram is a binary eutectic system with high solid solubility (see Figure 1.2). Silver also has excellent physical and mechanical properties for an interlayer material. It is ductile and relatively weak (YS = 55 MPa and UTS = 125-130 MPa). Its oxide becomes thermally unstable at 210 °C and 1 atm [8]. At an oxygen partial pressure of 0.20 atmospheres (in air), silver oxide is thermally unstable above 190 °C [9]. Since 190 °C is a homologous temperature of only 0.38 for silver, it is possible to bond oxide-free surfaces below 0.5 T_m of silver. Thermodynamic stability data for silver and copper oxides at several temperatures [8] and the

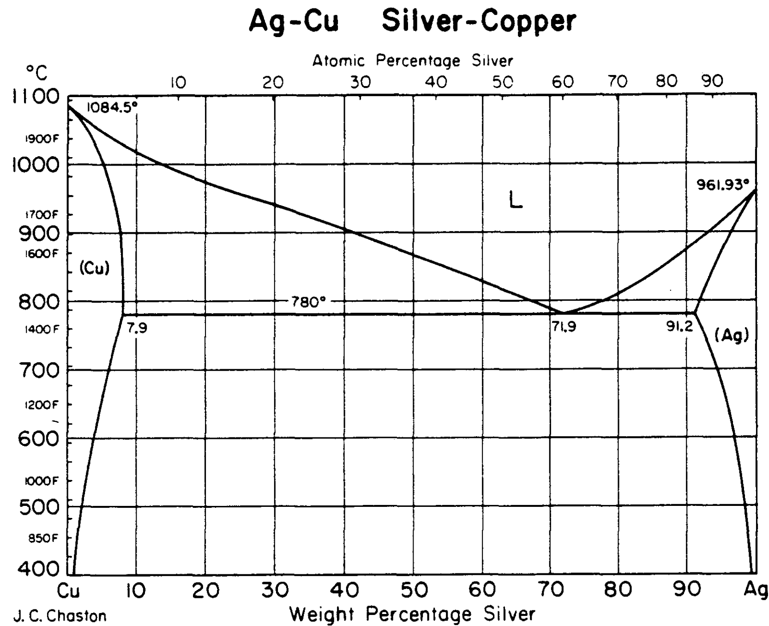

Source: Metals Handbook, vol. 8, p. 253 (1973).

Figure 1.2: Copper-silver binary phase diagram.

corresponding equilibrium oxygen partial pressures are given in Table 1.1. The importance of oxide removal for metal to metal contact was shown by Mohomed and Washburn [4]. They found that the loss in bond strength for several metals correlated with the increase in hardness of a metal oxide relative to the hardness of the metal itself. The relative hardness for several metals and their oxides is given in Table 1.2. Finally, there is a large bonding data base for silver interlayers. Gold has better oxidation behavior (ΔG_f for Au_2O is

Table 1.1: Free energy of formation and equilibrium partial pressure of oxygen at several temperatures for silver and copper oxides.

T	$4 Ag + O_2 \rightarrow 2Ag_2O$		$2Cu + O_2 \rightarrow 2CuO$		$4Cu + O_2 \rightarrow 2Cu_2O$	
(°C)	ΔG°_f (KJ/mol)	$p^{eq}_{O_2}$ (torr)	ΔG°_f (KJ/Mol)	$p^{eq}_{O_2}$ (torr)	ΔG°_f (KJ/mol)	$p^{eq}_{O_2}$ (torr)
20	-24	0.05	-256	10E-43	-288	10E-49
100	-14	10	-243	10E-31	-277	10E-36
150	-7	100	-234	10E-26	-269	10E-31
190	-2	300	-227	10E-23	-263	10E-27
210	0	760	-223	10E-22	-261	10E-25
300	+12	8500	-208	10E-16	-247	10E-20
1050*	NA	NA	-79	0.09	-139	10E-4

*Near melting point of copper
Source: Rosenquist [8]

Table 1.2: Relative hardness of several metals and their oxides.

Metal	Hardness (HV)	Oxide	Hardness (HV)
Al	15	Al_2O_3	1800
Cu	40	Cu_2O	160
Ag	26	Ag_2O	135
Au	20	--	--

Source: H.A. Mohamed and J. Washburn [4].

positive at room temperature) and it is more ductile. However, it is very expensive and so there is very little existing bonding data for gold interlayers.

Much of the previous data for solid-state bonding with silver interlayers involves foils, electrodeposited coatings or vapor deposited coatings. Knowles and Hazlett [10] used electrodeposited silver interlayers to bond berylium. They observed a linearly increasing strength versus thickness for a plating thickness range of 0.8 μm to 15 μm (30 μin to 580 μin).

Dini, Kelley, Cowden and Lopez [11] electroplated silver on stainless steel, berylium and uranium. For type 304 stainless steel, they found that the bond strength decreased from 385 MPa (56 ksi) to

165 MPa (24 ksi) as the thickness was increased from 25 μm to 75 μm at a bonding temperature of 300 °C. The berylium and uranium bond strengths showed no thickness dependence under the same conditions.

Electrodeposited silver coatings have also been used to successfully bond aluminum alloys [6,12] and aluminum to stainless steel [13]. In bonding these alloys, special joint preparations were necessary to confine the deformation to the joint. Cline [6] achieved bond strengths of up to 110 MPa (16 ksi) by bonding at 370 °C for 30 minutes. The total deformation under these conditions was 50 percent. Barta [12] achieved joint shear strengths of 46 MPa (6700 psi) at 230 °C and 25 MPa (3600 psi) at 150 °C. A bonding pressure of 110 MPa (16,000 psi) was applied for four hours. Crane, Lovell, Baginski and Olsen [13] successfully bonded 2219 aluminum to type 316 stainless steel. They found that the optimal conditions were 260 °C (500 °F) for 2 to 4 hours. Their corrosion tests showed that diffusion welded silver joints would require a coating if the joints were exposed to an electrolyte such as water or condensate.

Macleod and Mah [14] used a hot-hollow cathode (HHC) deposition technique to deposit silver on stainless steel. They found that the bond strength reached a peak for a certain substrate bias voltage. Naimon et al [15] used a similar method to join berylium to berylium and aluminum to aluminum. The berylium joints nearly always failed in the base metal. The Al-Al joints failed at the Al-Ag

ARTHUR LAKES LIBRARY
COLORADO SCHOOL of MINES
GOLDEN, COLORADO 80401

interface until a threshold value for total ion bombardment cleaning energy was reached. There results were inconclusive as there was a wide range of bond strengths.

Naimon, Doyle et al [16] observed that the formation of thick intermetallics led to a decrease in bond strength and a major loss of impact strength. Calderon, Walmsley, and Munir [17] found that the bond strength decreased linearly with the square root of the thickness of the intermetallic. Both groups of researchers used HHC deposition techniques to coat type 316L stainless steel and 1100 aluminum. They found that lowering the bonding temperatures produced stronger bonds due to the avoidance of the formation of Ag_2Al and Ag_3Al.

Most of the previous workers varied thickness or bonding parameters such as time, temperature, and pressure. Schalansky, Munir and Walmsley [18] studied the effect of coating parameters on the adhesion of HHC deposited silver on type 304 stainless steel. They found that at low substrate temperatures (120 °C) a porous columnar structure was formed, while at moderate temperatures (530 °C) densely packed columnar grains were formed. The bond strength increased slightly for increased coating substrate temperatures, and greatly increased for higher coating angles of incidence (the angle between the incoming silver atoms and the stainless steel substrate).

D. Sputter Coating

Sputtering is a physical process in which atoms are removed from a material. Sputtering is a fairly well understood process. It has been reviewed by Chopra [19], Westwood [20], Holland [21] and Winters et al. [22]. In this process, momentum is transferred from an incident energetic particle (usually an ion) to atoms of the target material. When the target is a material which is to be cleaned or etched, it is called sputter cleaning or sputter etching. When the sputtered atoms are implanted into another substrate, it is called sputter deposition. These sputtered atoms typically have an average energy of 5 to 30 eV. Usually argon or another noble gas is positively ionized since their energy (and thus their momentum) can be controlled by applying a potential to the target. Magnetron sputtering is the most widely used because it is possible to get high current densities which provide higher deposition rates and because it has a flexible geometry. In magnetron sputtering, a magnetic field is applied by a fixed magnetic pole near the target which imparts a helical motion to the electrons of the plasma. This leads to an increase in path length which causes an increase in the number of ionizing collisions and the plasma density [22]. In addition, there is also a reduction in the number of secondary electrons which reach the substrate after they eject from the target so that substrate heating is reduced considerably.

Sputter deposition offers several advantages over other deposition techniques [22]. It can be used for almost any material if a suitable target can be fabricated. However, iron cannot be deposited using magnetron sputtering because of the nature of the magnetic field. Generally, there is a more uniform thickness and better composition control than with other deposition techniques. In addition, compounds and multi-element materials can be sputtered. Adhesion is also improved by using sputter deposition techniques. The higher kinetic energies of the sputtered atoms lead to a greater mechanical interlocking between the substrate and the incoming atoms. Finally, the system can be designed so that the substrate can be sputter cleaned before or even during sputter deposition. This makes it possible to coat before oxides have time to reform on the surface. Cathode-vapor deposition is the only other coating technique where this is possible.

Four distinct growth modes have been observed in sputter coating [20]. The growth mode is a function of both the homologous temperature and the sputtering pressure (or the energy/deposited atom). Figure 1.3 is a zone diagram showing the film morphology as a function of these parameters. This diagram can be applied to both sputtered and evaporated films. The major difference between sputtered and evaporated films is that evaporated films are normally under tensile stress while sputtered films are usually in compression

because of "atomic peening" by the energetic atoms as they hit the substrate.

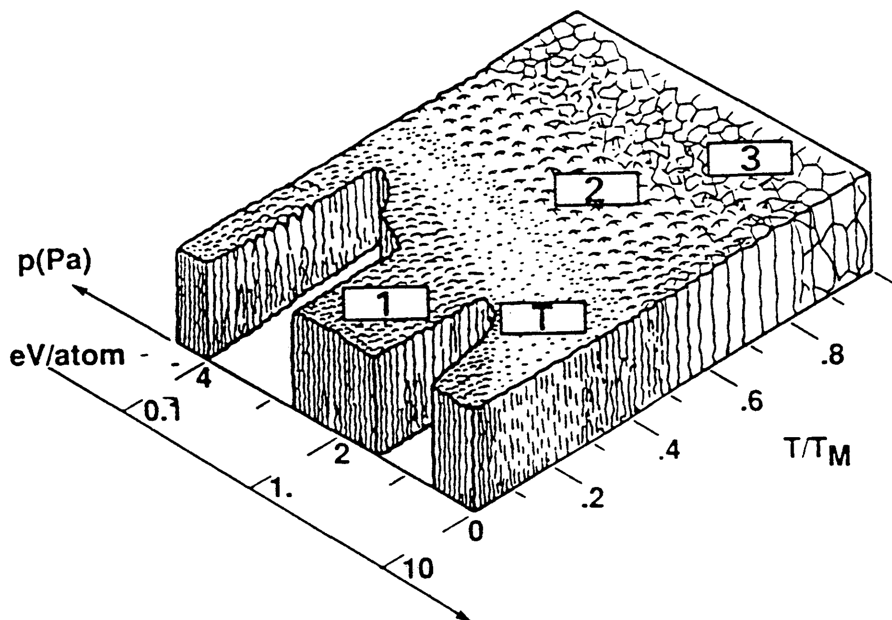

Source: Westwood [20]

Figure 1.3: Zone diagram for sputter deposition. Film morphology is shown as a function of homologous temperature and sputtering pressure.

The atomic processes occuring in each zone of the diagram are discussed by Westwood [20]. At low temperatures (zone 1), the atoms reach a cold substrate with very little energy which results in a film consisting of individual columns separated by voids. As the temperature or sputtering pressure is increased, the films become

denser and have specular surfaces (zone T). This is the type of morphology which is expected for most metals when sputtering is done at room temperature. When the temperature or energy is increased even further, grain growth occurs and dense films with rough surfaces are observed. Finally, at very high temperatures (0.8 to 1.0 T_m) bulk diffusion occurs and classical polycrystalline materials are obtained (zone 3). This zone is at a higher temperature than typical sputtering operations.

The film structure is also dependent on substrate material, substrate motion and film thickness [19,23,24,25]. Nieh and Wadsworth [23] used vapor deposition and sputter deposition to produce thick magnesium and beryllium foils (0.75 mm thick). The adhesion of magnesium was much lower for a carbon substrate versus a stainless steel or magnesium substrate. A highly isotropic columnar structure was observed which could be modified by replacing the stationary substrate with a moving one. For a rotating substrate, helical columnar grains were formed. For beryllium, this led to an increase in the in-plane microyield strength from 35 MPa to 168 MPa.

Lee [24] sputtered thin chromium films on NaCl single crystals, Al and Ni-P polycrystals and Na_2O glass. They always observed only a (110) oriented texture regardless of substrate material or film thickness. This is not true of all materials. Chopra [19] lists many examples where preferred orientation is dependent upon the target material, the substrate material and the substrate temperature.

Lee [24] also observed an increase in columnar grain size with increasing thickness. Jankowski and Wilford [25] observed a similar increase in columnar grain size with thickness for vapor deposited titanium coatings. However, they observed a critical thickness (25 μm), above which the grain size stabilizes. At this thickness, they observed a (0002) preferred orientation of 7 (where 10 corresponds to a coating with all of its grains oriented (0002)).

II. Experimental Procedure

The experimental procedure consisted of several steps. First, all of the samples were machined to the same nominal surface roughness (Ra = 0.25 ± 0.12 μm). The machined surfaces were sputter coated with several thicknesses of silver using several deposition rates. One sample from each coating run was reserved for X-ray diffraction and SEM analysis. Another sample was cross-sectioned for coating thickness measurements. The rest of the samples were bonded in pairs under the same bonding conditions. These samples were turned down on a lathe and tensile tested. Finally, at least one fracture surface from each coating condition was examined using the SEM.

A. Sample Machining

The bonding specimens were machined from 12.5 mm (0.5 in.) diameter rods of electrolytic tough pitch (ETP 110) copper. This material has a wide range of mechanical properties depending on the degree of cold-work. The ultimate tensile strength ranges from 220 MPa for fully annealed rod to 340 MPa for maximum cold-working. This corresponds to a hardness range of R_F 40 to 90. The mechanical properties are shown in Table 2.1 along with the chemical composition of this alloy.

The bonding specimens were right circular cylinders. One end was turned down to a diameter so that when two samples were

Table 2.1: Mechanical properties and chemical composition of electrolytic tough pitch copper (ETP 110).

Mechanical Properties			
Form or Condition	Tensile Strength (MPa)	Yield Strength (MPa)	Rockwell F Hardness
soft (G.S.= 0.050 mm)	220	69	40
soft (G.S.= 0.025 mm)	230	76	45
1/8 hard	250	190	60
1/4 hard	260	210	70
1/2 hard	290	250	84
hard	340	310	90

Chemical Composition	
Element	Amount Present
Cu (+Ag)	99.9 %
Ag	0.102 % (counted as copper)
O	0.01 - 0.07 % (nominal 0.04 %)
Pb	< 0.005 %
others	may be present in small amounts

Source: ASME Handbook: Metals Properties, New York, p. 300 (1954).

bonded, a standard round tensile bar was formed. A schematic of the bonding coupon is shown in Figure 2.1.

The sample surfaces were prepared using a milling technique developed by Nicholas [26] and Nichting [27]. The bonding surfaces were machined on a vertical mill using a single-point milling cutter with a carbide tip, producing a finished surface comprised of rows of nearly parallel ridges with the same height and peak-to-peak spacing. Milling is a major improvement over lathe machining, where the machine feed rate changes as the cutting tool moves towards the center of the sample, resulting in a gradient in roughness and a variation in peak-to-peak spacing. It is also better than surface grinding which can lead to smearing, irreproducible roughness and surface contamination from the grinding materials. Nicholas [26] and Nichting [27] have shown that by controlling the mill speed and the table speed, a consistent copper surface roughness can be achieved. Figure 2.2 shows a cross-section of a sample with a surface roughness of R_a = 1.1 μm (43 μin). Both the peak-to-peak spacing and the peak heights are very consistent. This sample was machined at a fast table speed (1.7 mm/s) and a slow mill speed (8.3 rps) which results in a very rough surface. For the actual experimental runs, a very fine surface finish was desired so a table speed of 0.63 mm/s and a mill speed of 67 rps was used. This produced a nominal surface roughness of R_a = 0.25 μm ± 0.12 μm (10 ± 5 μin).

Before Bonding:

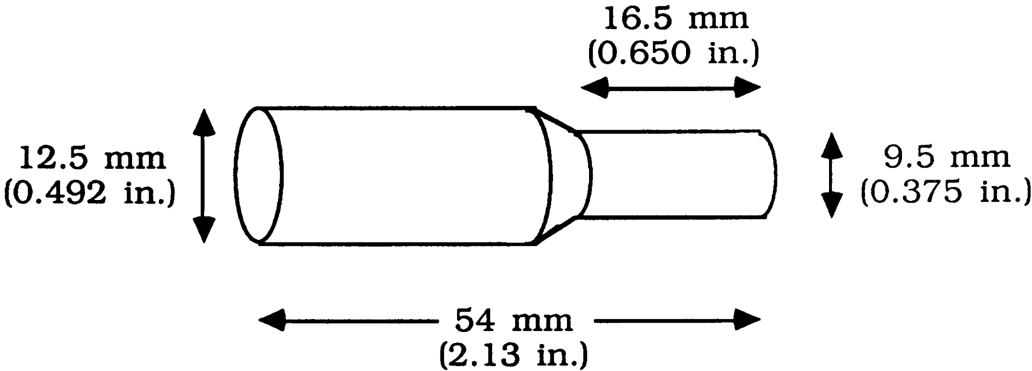

After Machining for Tensile Testing:

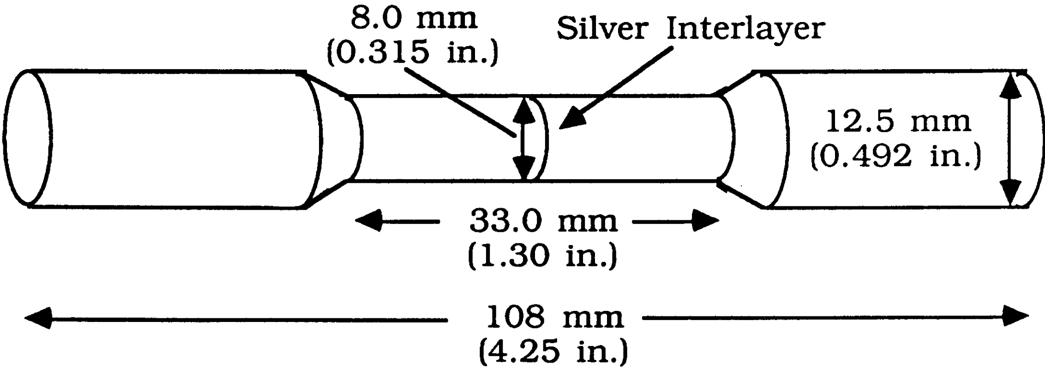

Figure 2.1: Schematic of bonding coupons showing the sample dimensions prior to bonding and prior to tensile testing.

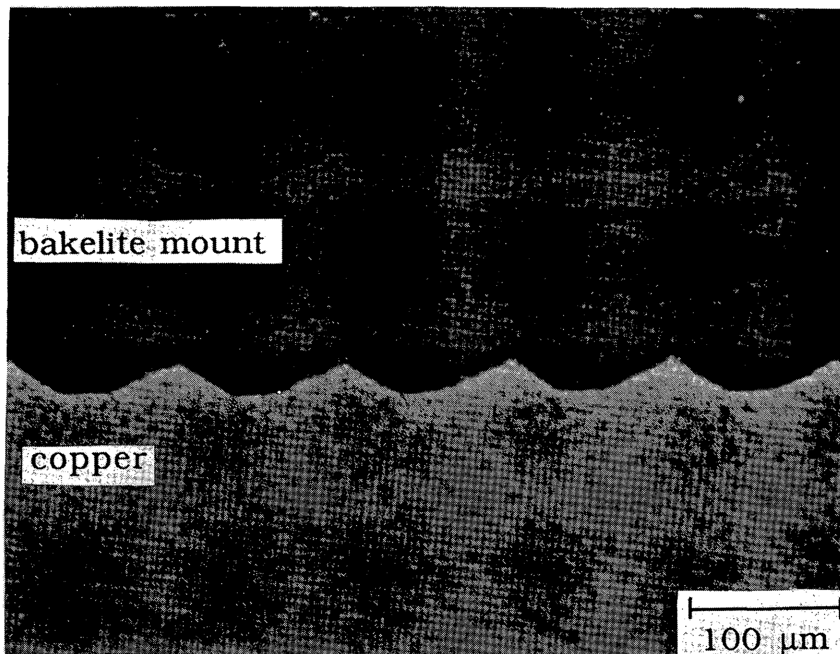

Figure 2.2: Cross-section of an as-machined copper surface with an average roughness of 1.1 μm (43 μin) (200X).

B. Coating Procedure

Prior to coating, the machined samples were ultrasonically cleaned for ten minutes in acetone to remove any lubricants and dirt left on the surface during machining. Next, the samples were ultrasonically cleaned in methanol for ten minutes to remove any acetone residue on the bonding surfaces. After cleaning, the samples were blown dry with dichlorofluoromethane to minimize methanol residue on the bonding surface.

The bonding surfaces were coated with 1 μm to 43 μm (39 μin. to 1700 μin.) of pure silver (99.9 wt. pct.) using an inverted magnetron sputter coating unit. A schematic of this unit is shown in Figure 2.3. The unit has a magnetron sputtering gun with a 50 mm (2 in.) target and a variable speed rotating sample holder which can hold up to 20 samples. The samples can be connected to a bias voltage power supply if sputter cleaning is desired. The chamber has inlets connected to a high vacuum diffusion pump, a mechanical pump, an argon bleed system and an ion gauge. Ten samples were loaded into the sample holder and the chamber was pumped down to a nominal vacuum of 5×10^{-5} torr. Then research grade argon (99.998 pct.) was bled into the system so that an argon pressure of 30 ± 10 mtorr was maintained. Next, the samples were sputter cleaned for 15 minutes at a bias voltage of 2000 V. This assists the removal of surface oxides and contaminants which hinder the intimate metal-metal contact desired for improved coating adhesion.

After cleaning the sample surfaces, the bias voltage was removed and silver was sputtered onto the surface from a target located 50 mm (2 in.) from the samples. The sample holder was rotated at approximately 0.05 rps so that a given sample was exposed to one second of sputtering followed by 19 seconds with no sputtering. The deposition current and time were varied to get several thicknesses and coating morphologies. Current and time were chosen as variables because thickness varies linearly with both of these parameters.

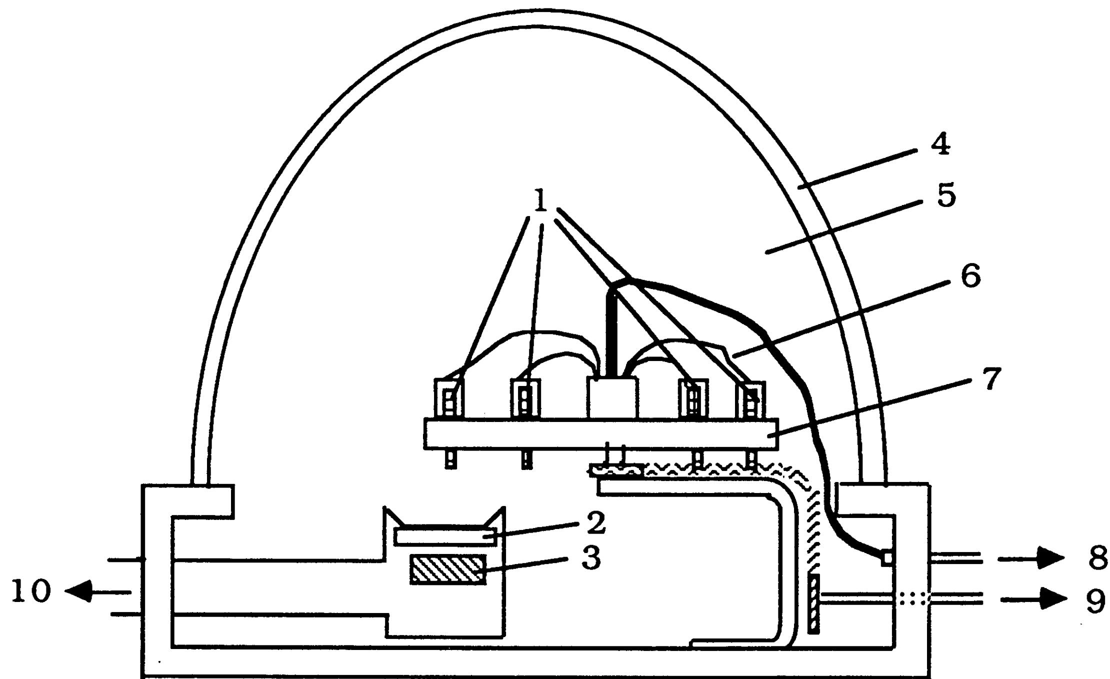

1. Samples (20 max)
2. Silver Target
3. Cylindrical Magnet
4. Vacuum Bell Jar
5. High Vacuum Chamber
6. Electrical connections for Bias Voltage
7. Rotating Sample Holder
8. To Bias Voltage Power Supply
9. To Sample Holder Drive Motor
10. To Sputter Gun Power Supply

Not shown: Outlets to diffusion pump, mechanical pump and argon bleed valve.

Figure 2.3: Schematic of inverted magnetron sputter coating unit.

Therefore, it was possible to get the same thickness for several currents. Deposition power or voltage could have been varied but this would have made it difficult to predict the resulting thickness. The coating conditions are summarized in Table 2.2. The samples never heated above 40 °C during coating and could be touched immediately after coating.

Table 2.2: Coating Parameters.

Coating Material:	Pure Silver
Sputter Cleaning:	2000 V for 15 min.
Nominal Vacuum:	2×10^{-5} torr
Argon Pressure:	20 to 35 mtorr
Sputter Current:	Variable (0.10 amps to 0.70 amperes)
Sputter Cycle:	1 second sputtering followed by 19 seconds without sputtering
Coating Time:	Variable (25 min. to 480 min.)
Coating Thickness:	Variable (1 μm to 43 μm)

C. Bonding Procedure

Prior to bonding, two coated samples were cleaned using a procedure similar to the one used before coating. The samples were ultrasonically cleaned for ten minutes in acetone and for ten minutes

in methanol. Then the samples were blown dry with dichlorofluoromethane.

A thermocouple was spot-welded onto the side of the sample approximately 1 cm (0.4 in.) from the coated end. The samples were then loaded into the bonding chamber which is shown schematically in Figure 2.4. A stress was applied using a standard Instron mechanical testing machine with a creep cage and modified compression grips. The machining ridges on the two surfaces were aligned perpendicular to each other so that the initial number of peak to peak contact points was maximized. The chamber was pumped down to a nominal vacuum of 5×10^{-6} torr. When the desired vacuum was achieved, the coupons to be bonded were brought together under a nominal compressive stress of less than 5 MPa. Unlike the previous work done by Nicholas [26] and Nichting [27] for copper-copper bonding, no sputter cleaning was necessary since silver dissolves its own oxide at 210 °C (483 K) and 1 atm O_2 [9]. Instead, the samples were immediately heated to 300 °C (573 K) using an induction heating coil. The heating cycle lasted 600 to 900 seconds. When the temperature reached 300 °C, the bonding pressure was increased to 70 MPa (10 ksi). The pressure was maintained for an 1800 second (30 minute) isothermal stage and then the samples were allowed to air-cool down to room temperature. The cooling cycle lasted 2700 to 3600 secondss. The load was not removed until the bonded samples had cooled below 40 °C so that residual tensile stresses which could

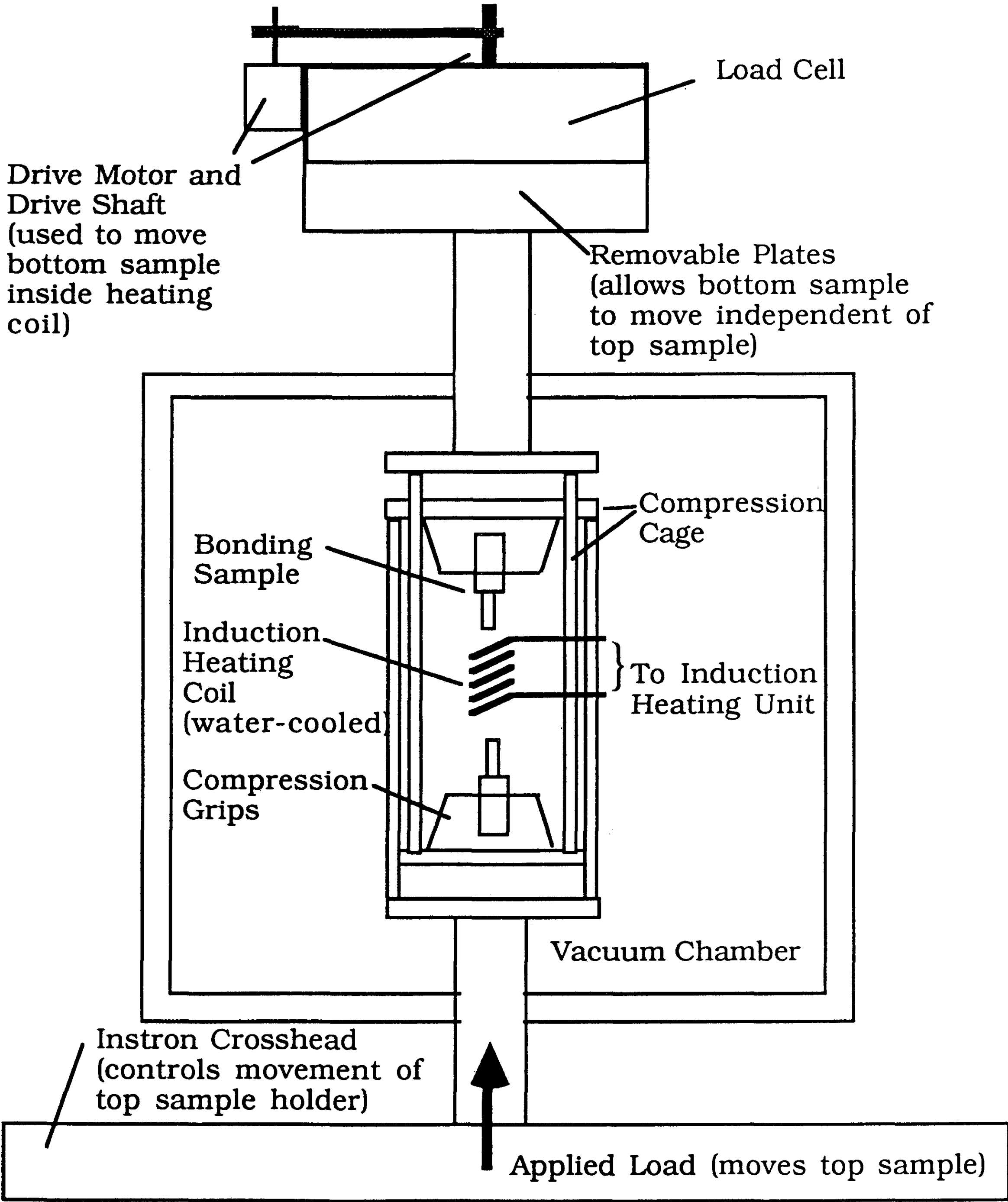

Figure 2.4: Schematic of bonding unit.

be created at the joint due to thermal contraction during cooling were avoided. The bonding conditions are summarized in Table 2.3.

Table 2.3: Bonding Parameters.

Bonding Temperature:	300 °C (573 K)
Bonding Pressure:	65 MPa (10 ksi)
Nominal Vacuum:	5 X 10^{-6} torr
Heat-up Cycle:	600-900 seconds (10-15 min.)
Time at Temperature:	1800 seconds (30 min.)
Cool-down Cycle:	1200-2400 seconds (20-40 min.) with bonding pressure still applied

D. Mechanical Testing

After bonding, the reduced diameter section of the sample was turned down to nominal diameter of 7.9 ± 0.1 mm (0.315 ± 0.005 in.) to eliminate notch effects and bending moments introduced by mismatch between the bonding surfaces. All of the samples were machined to the same diameter so that the thickness to diameter ratio was constant for a given thickness. The samples were loaded to failure in tension at a displacement rate of 0.02 mm/s (0.05 in/min) using a standard Instron testing system. The bond strength was either the maximum engineering stress reached for samples which failed in

the joint or the ultimate tensile strength of copper for samples which failed completely within one copper tensile-half specimen.

E. Thickness Measurements

One sample was saved from each coating run for coating thickness measurements. This sample was cross-sectioned, mounted in bakelite, and polished. The thickness was measured using a light microscope. Although there was some smearing of the silver cross-section during polishing due to the softness of the silver relative to the copper, the thickness measurement was accurate to ± 1 μm. When failure occurred by copper-silver de-adhesion, it was possible to check the coating thickness on the SEM. The thickness measurements on the SEM were found to be in very good agreement with those measured using the cross-sectioned samples.

F. Microstructural Examination

A second sample was saved from each coating run for microstructural examination. X-ray diffraction tests were run on this sample for preferred orientation measurements and SEM surface evaluation was performed in order to characterize the coating morphology. After bonding, fracture surfaces were examined using the SEM.

G. Test Matrix

Preliminary coating runs were done at deposition sputter currents of 0.10, 0.40 and 0.70 amperes. At the extreme ranges (0.10 and 0.70 amperes), the power unit had difficulty maintaining a steady current. This made reproducibility and prediction of of thickness impossible. In addition, long coating times ($\geq$ 8 hrs) were required even for the thin coatings at 0.10 amperes. Therefore these current extremes were abandoned. However samples from the preliminary runs were examined if they fell within the desired thickness ranges.

The final test matrix was a 3 X 3 matrix consisting of 3 currents (0.20, 0.40 and 0.55 amperes) and 3 coating thicknesses (6 $\pm$ 1 μm, 13 $\pm$ 2 μm and 20 $\pm$ 3 μm). Additional runs were done in the thickness range of 1 μm to 43 μm to examine the thickness effect for very thin and very thick coatings. Extra coating runs were also done at several currents for a constant thickness of 20 $\pm$ 3 μm in an effort to get a wide range of microstructures in the optimal thickness range. The constant current test matrix is summarized in Table 2.4 and the constant thickness matrix is summarized in Table 2.5. Three to four bonds were made at each coating condition so that data scatter could be minimized.

A final coating run was done at 0.40 amperes in an attempt to lower the bonding temperature for the optimal coating thickness. All of the bonding conditions were held constant except that the temperature was lowered and the bonding pressure was increased. A

Table 2.4: Test matrix for constant current sputtered silver coatings showing the number of bonds for a given coating run.

Deposition Current (amperes)	Coating Thickness (μm)						
	1	2	6 ± 1	13 ± 2	21 ±3	35	43
0.20	-	-	4	4	4	-	-
0.40	4	3	4	4,1*	4,1*	3	3
0.55	-	-	4	4	4	-	-

* Two coating runs

Table 2.5: Test matrix for constant thickness sputtered silver coatings showing the number of bonds for a given coating run.

Coating Thickness (μm)	Sputter Deposition Current (amperes)								
	0.10	0.20	0.30	0.35	0.40	0.45	0.50	0.55	0.70
6 ±1 μm	2	4	-	-	4	-	-	4	2,2*
13 ± 2 μm	2	4	-	-	4,1*	-	-	4	-
21 ± 3 μm	-	4	4	4	4,4*	4	4	4	-

* Two coating runs

20-μm-thick coating was applied and the samples were bonded under the following conditions:

Temperature (°C)	Pressure (MPa)	Number of bonds
300	65	3
220	100	2
220	125	1
150	125	2
150	165	1
100	145	1

III. Results and Discussion

The evaluation of the silver interlayers was divided into four major sections. In each section, both the effects of coating thickness (constant deposition current) and sputter deposition current (constant thickness) were examined. In the first section (A. Bond Strength Measurements), the effects of thickness and deposition current on bond strength were examined. The effects of bonding pressure and temperature on bond strength were also discussed. In the second section (B. Crystallographic Orientation of Sputtered Coatings), the preferred orientations of the coatings and the relation between bond strength and preferred orientation were discussed. The next section (C. Microstructure), presents the different coating morphologies which were observed. The final section (D. Fracture Surface Examination), compares the fracture surfaces for different interlayer thicknesses and bond strengths.

A. Bond Strength Measurements

The samples had bond strengths which ranged from 50 MPa to 255 MPa. Thickness was the most important factor in determining bond strength. The sputter deposition current was only a factor for thin coatings. All of the samples were bonded for 1800 seconds at 300 °C and a bonding pressure of 65 MPa (10 ksi) with the exception of the samples from the last coating run which were bonded for 1800 seconds at several different temperatures and bonding pressures.

The samples had a hardness range of R_F = 60 to 85 which corresponds to an ultimate tensile strength of between 230 and 250 MPa. Several of the samples failed completely within a copper tensile half, displaying an ultimate tensile strength of between 230 and 250 MPa, which is slightly lower than the hardness measurements predicted. When the temperature was decreased, full strength bonds could not be achieved even when the optimal coating conditions were used.

A.1. Effect of Thickness on Bond Strength

Figure 3.1 shows the bond strength as a function of thickness for a sputter deposition current of 0.20 amperes. As the joint thickness was increased from 12 μm to 47 μm, the maximum bond strength did not change significantly but the variation in measured bond strengths decreased. All of the bonds were at least as strong as the yield strength of the copper and several were in the range of the ultimate tensile strength. All of the samples failed within the silver interlayer.

The bond strength for the same thickness range and a deposition current of 0.40 amperes is shown in Figure 3.2. The maximum bond strength for a given thickness was approximately constant for the joint thickness range of 12 μm to 44 μm. A similar decrease in the range of measured bond strengths with increasing coating thickness occurred, but at 12 μm the variation in measured bond strengths was much greater for the 0.20-ampere coating than for

ARTHUR LAKES LIBRARY
COLORADO SCHOOL of MINES
GOLDEN, COLORADO 80401

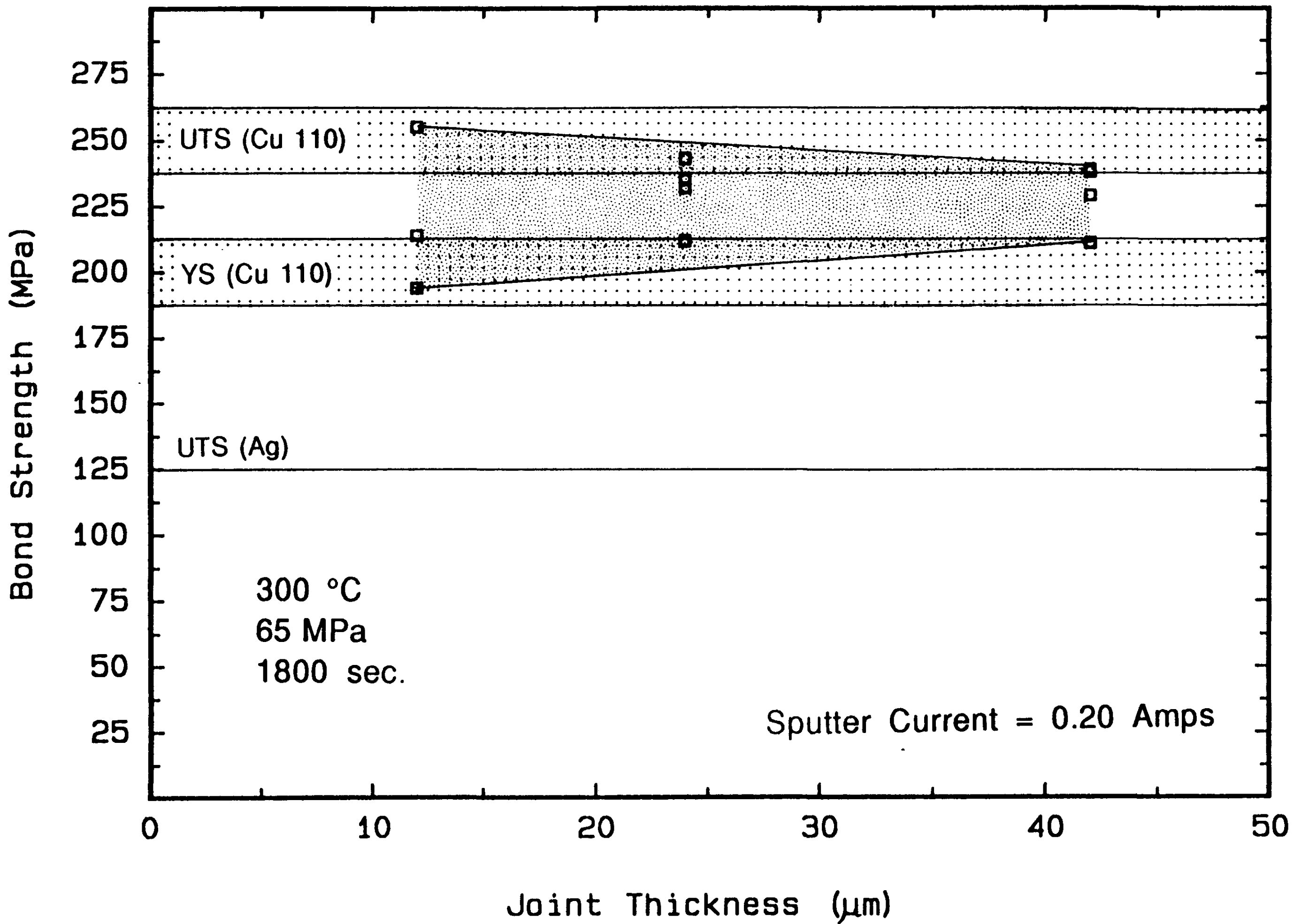

Figure 3.1: Bond strength as a function of joint thickness for a sputter deposition current of 0.20 amps.

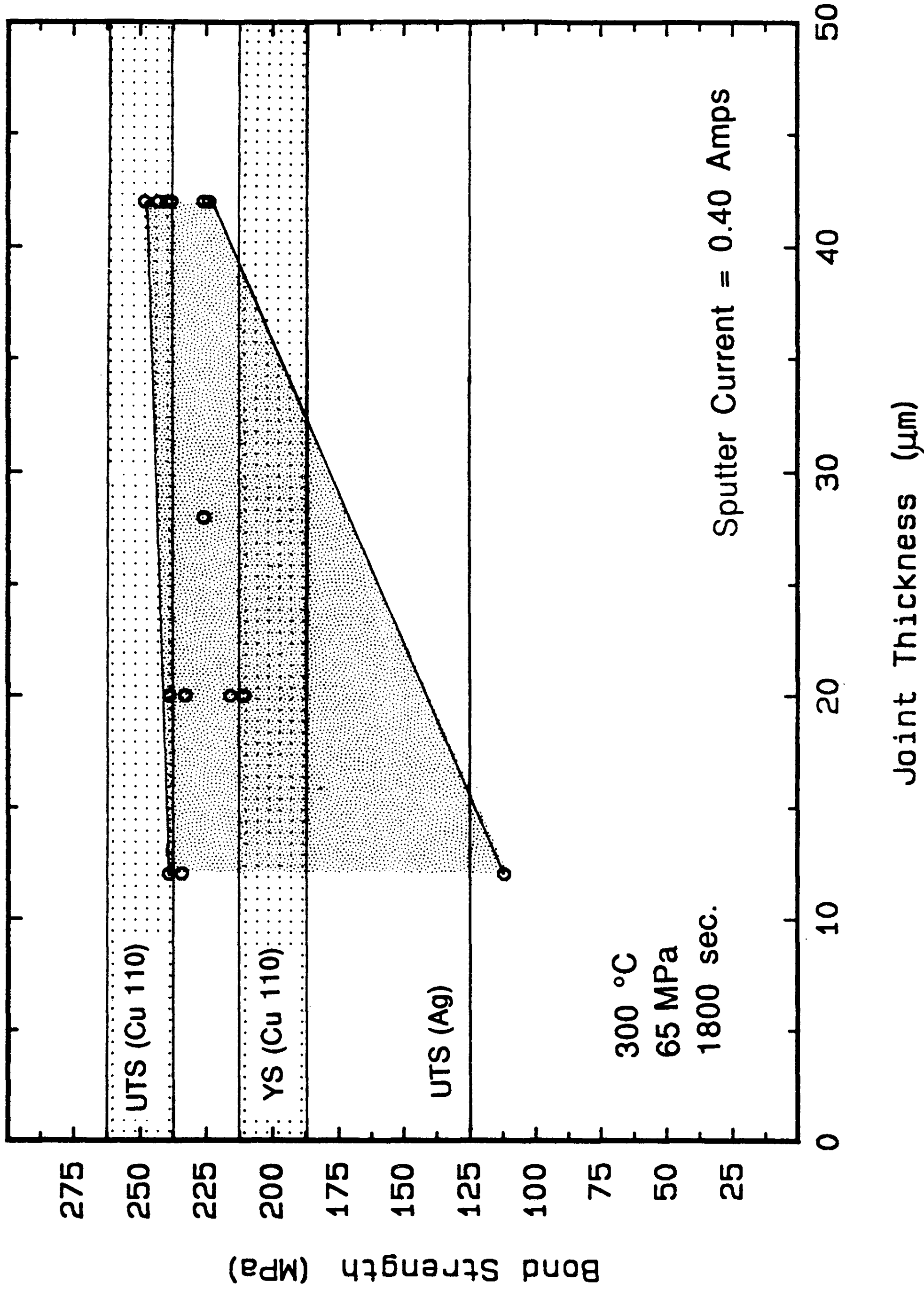

Figure 3.2: Bond strength as a function of joint thickness for a sputter deposition current of 0.40 amps.

the 0.40-ampere coating. Most of the bonds were above the yield strength range of the copper and some were in the ultimate strength range. However, one of the 12-μm-thick joints failed below the ultimate tensile of silver. All of the samples failed at the joint except two of the 44-μm-thick joints which failed in the copper substrate.

Figure 3.3 shows the bond strength versus joint thickness for a 0.55 ampere sputter deposition current. Again there is not a major change in the maximum bond strength for a given joint thickness in the range 12 μm to 40 μm. There is also a similar decrease in the range of measured bond strengths with increasing thickness. For this deposition current, all of the samples failed at the joint except for one 40-μm-interlayer bond which failed in the copper substrate. Only two bonds with a joint thickness of 12 μm failed below the yield strength range of the copper, and several of the bonds failed in the ultimate strength range of the copper.

The bond strength versus thickness is shown for an extended thickness range in Figure 3.4. The joint thickness range was 2 μm to 86 μm and the deposition current was 0.40 amperes. In this thickness range, there were three major regions of bond strength behavior. In region I (joint thickness < 35 μm), there was a large amount of data scatter and a decrease in bond strength with decreasing thickness. A similar decrease in strength for thin coatings has been observed by several researchers. Bredz [28], and Bredz and Schwartzbart [29], observed this phenomenon in brazing. They

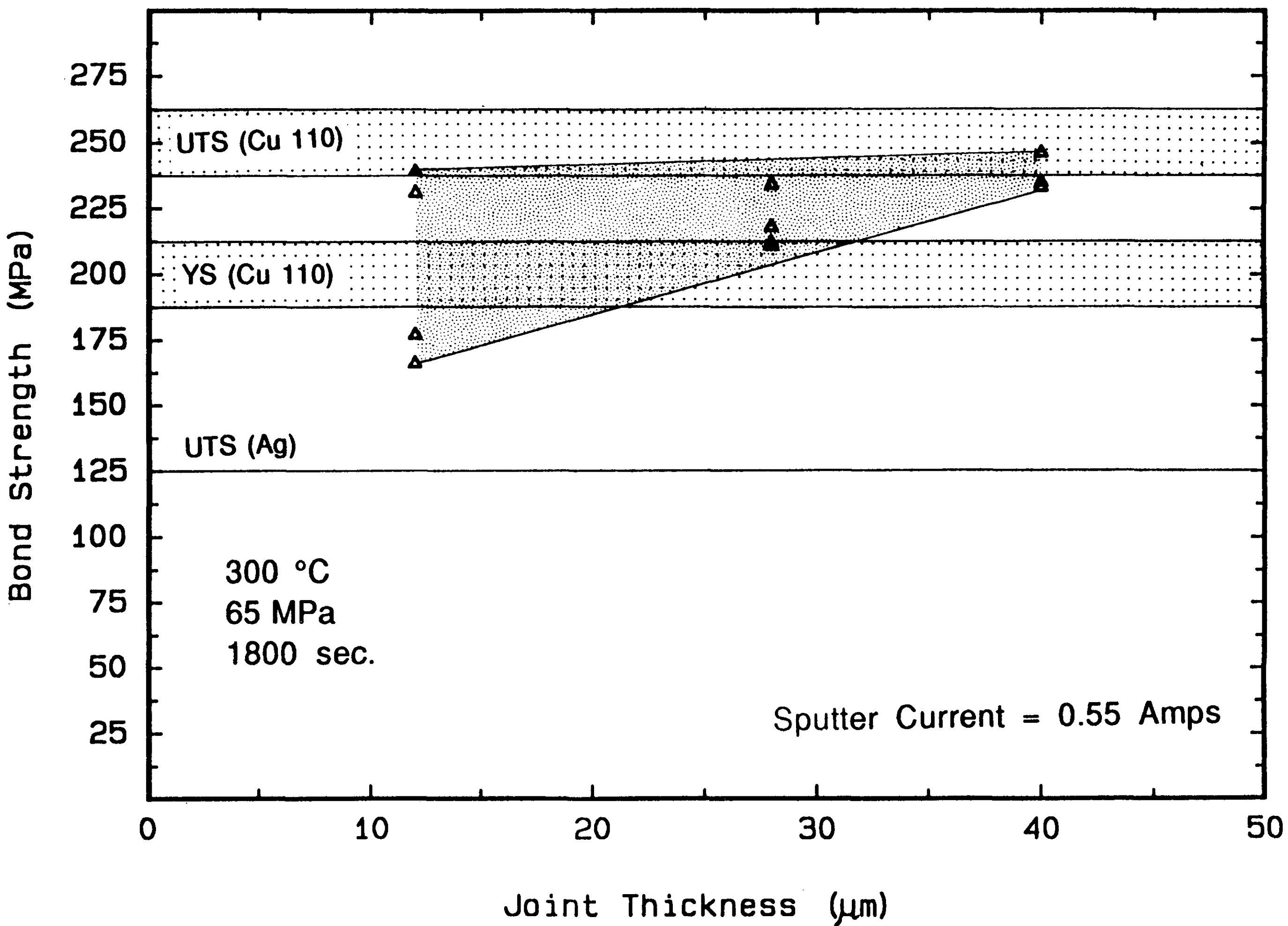

Figure 3.3: Bond strength as a function of joint thickness for a sputter deposition current of 0.55 amps.

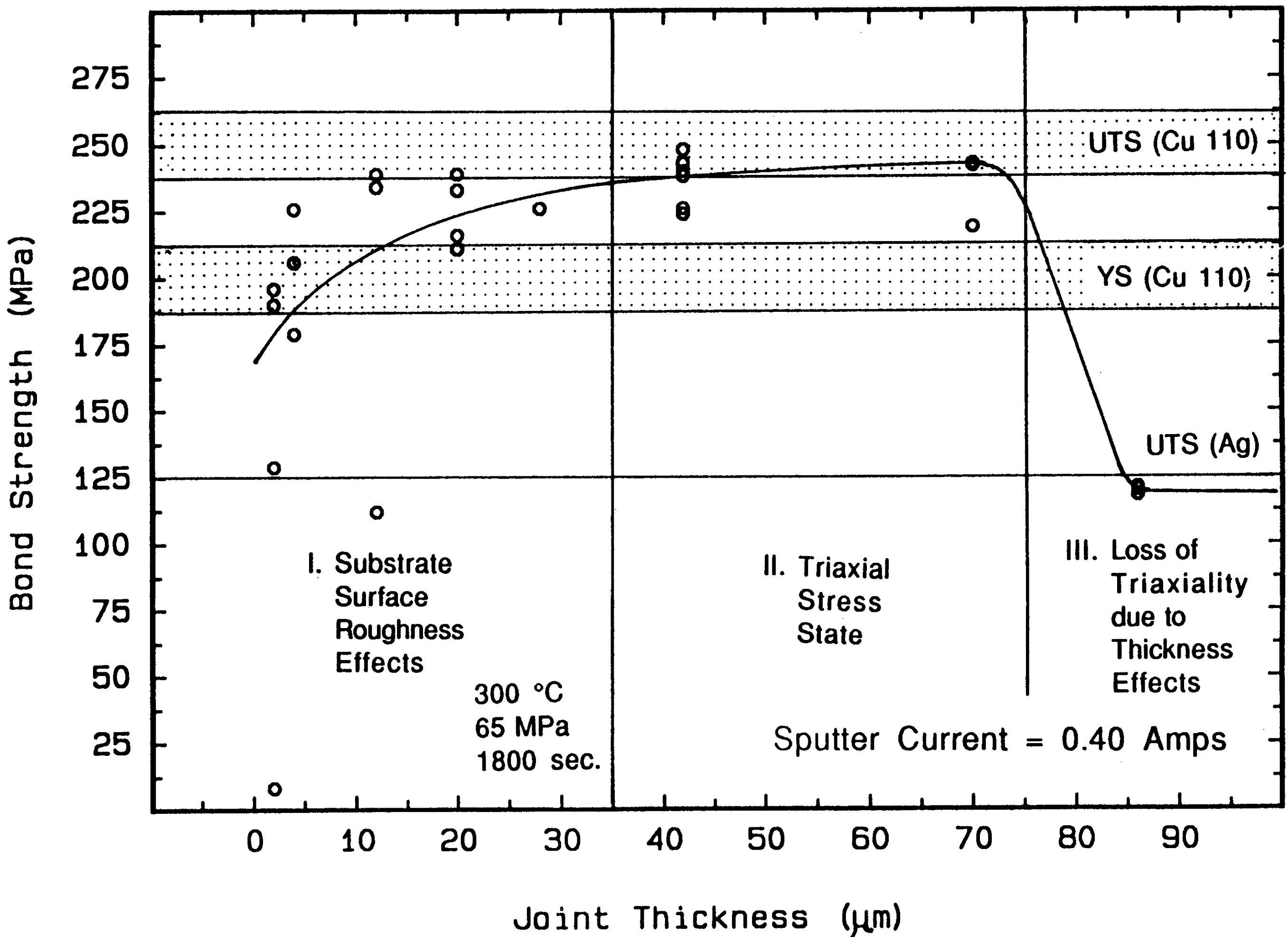

Figure 3.4: Bond strength as a function of joint thickness for a sputter deposition current of 0.40 amps and an extended thickness range.

attributed it to incomplete coating coverage of the substrate. However, sputter coating results in very uniform surface coverage even for very thin layers. This behavior was also observed by Knowles and Hazlett[10]; and O'Brien, Rice and Olson [30] in diffusion bonding. They attributed it to substrate surface roughness effects, which inhibit the plastic deformation of the interlayer. This is a reasonable explanation but it is surprising since this effect is observed at a coating thickness of greater than 15 μm when the surface has a nominal roughness of R_a = 0.25 μm.

In the thickness range of 35 μm to 70 μm (region II), high integrity joints were achieved. In this region, the variation in bond strength range for a given thickness is minimal and all of the bond strengths are above the yield strength range of the copper substrate. In this region, there is always enough plastic flow to achieve a sound joint and the substrate surface roughness has no effect. In addition, the joint is still thin enough to produce a high degree of triaxiality at the joint.

For the thicker joints in region III, the bond strength drops quickly to a constant value with increasing thickness. Above 70 μm, the bond strength is slightly less than the ultimate tensile stength of silver. In this range, the consistent bond strengths measured suggest that the necessary plastic flow is still occurring but that the triaxial stress state in the ductile interlayer is lost due to a loss of constraint with increasing thickness. Orowan's theory for brazed joints [7]

predicts a loss of triaxiality at 375 μm which is much higher than the observed 70-μm joint thickness. However, this theory assumed a perfect disc of ductile material between two infinitely rigid cylinders, while the copper in this study is relatively ductile. In addition, there are voids and non-bonded regions along the silver-silver bond line which could lead to stress concentrations inside the interlayer. Both of these factors would make a uniform triaxial stress state harder to achieve, thereby reducing the thickness at which triaxiality can be established.

A.2. Effect of Sputter Deposition Current on Bond Strength

Figure 3.5 is a plot of bond strength versus sputter deposition current for a joint thickness of 12 ± 2 μm. The current ranged from 0.10 to 0.70 amperes. At this joint thickness, the bond strengths ranged from 50 MPa to 250 MPa. This range is from less than one-half of the ultimate tensile strength of silver up to the ultimate strength of ETP 110 copper. Even though some of the samples had bond strengths in the ultimate tensile strength range of copper, all of the samples failed completely within the joint.

As the joint thickness was increased to 26 ± 4 μm, the variation in the measured bond strengths was dramatically decreased. Possible reasons for this increased consistency will be discussed in the next section. Figure 3.6 shows the bond strength versus sputter current for a current range of 0.10 to 0.55 amperes. All of the bond strengths

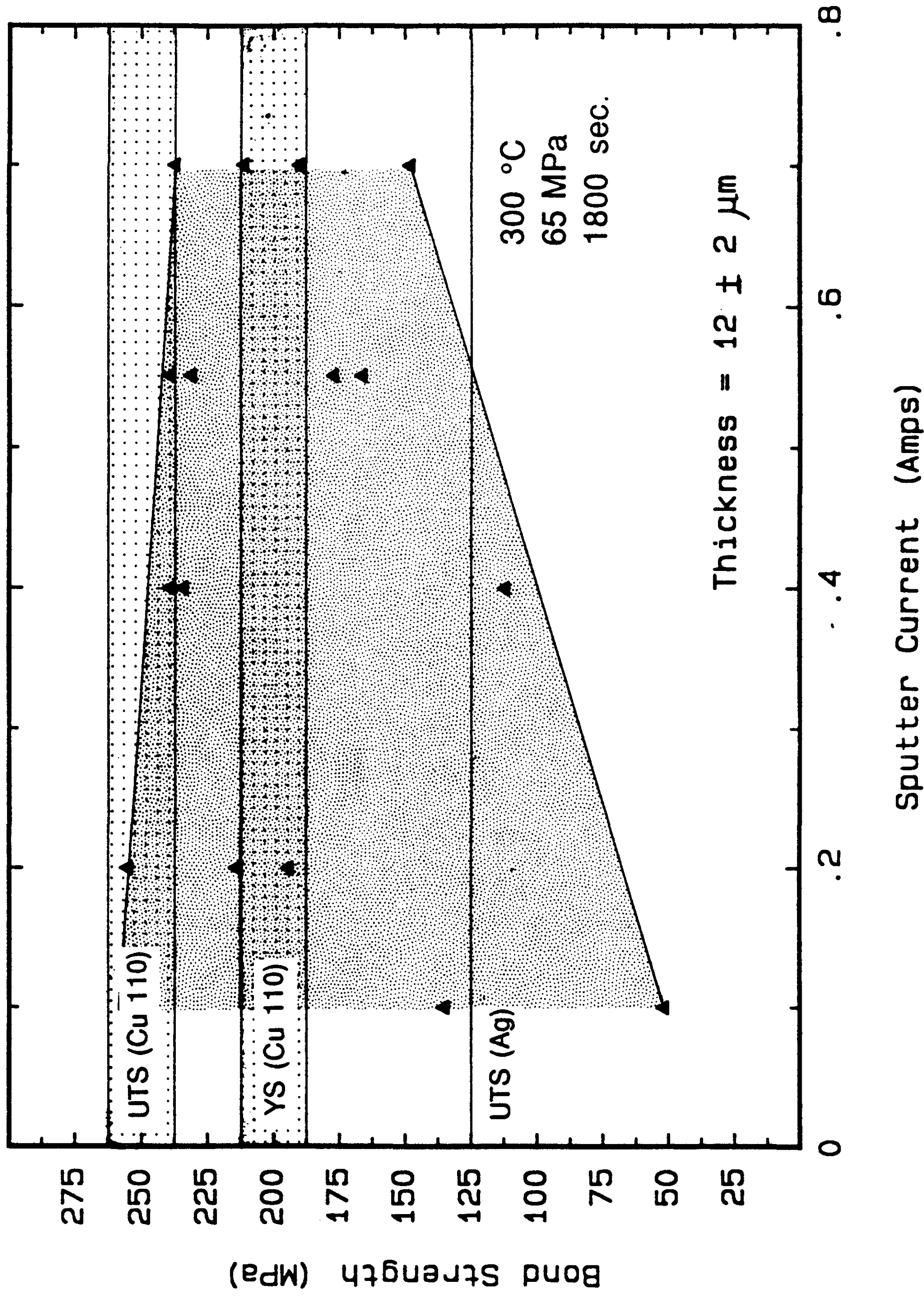

Figure 3.5: Bond strength versus sputter deposition current for a joint thickness of 12 ± 2 µm.

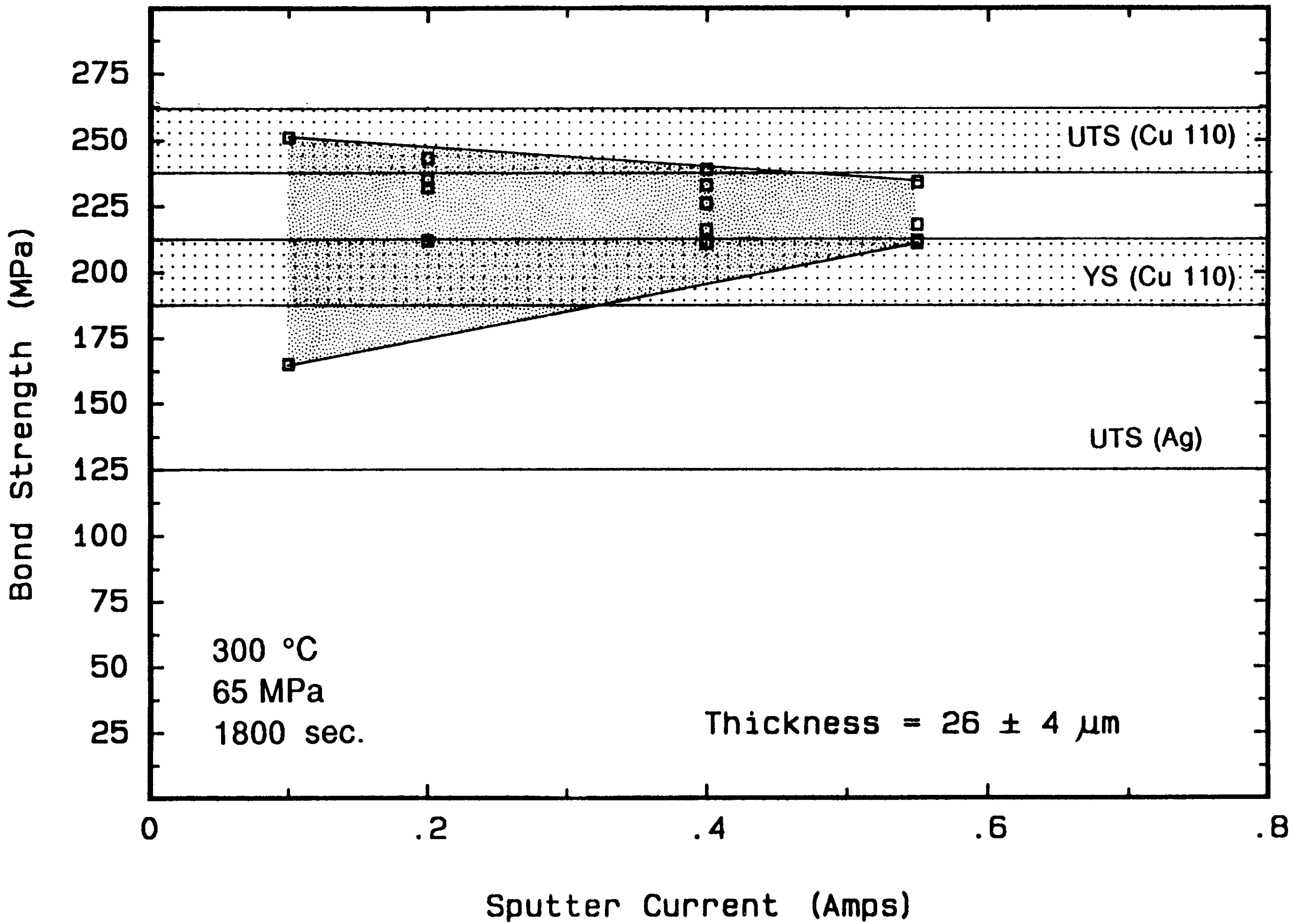

Figure 3.6: Bond strength versus sputter deposition current for a joint thickness of 26 ± 4 µm.

were higher than the ultimate tensile strength of silver and only one sample had a bond strength below the yield range of copper. All of the bonds failed at the joint except two which failed in the copper substrate.

When the joint thickness was increased to 41 ± 6 μm, very consistent and strong bonds were achieved. Figure 3.7 shows the bond strength for a sputter current range of 0.20 to 0.55 amperes. The bond strength had a range of 224 MPa to 247 MPa. Since the copper has ultimate tensile and yield strength variances of 20 MPa for the range of measured hardness values, the observed bond strength variance of 23 MPa is relatively small. In addition, the bond strengths are consistently higher than those at lower thicknesses. All of the bonds are above the yield strength range of copper and 11 out of 29 bonds failed in the copper. Even the bonds which failed in the silver interlayer had total gage length extensions of greater than 10 percent. This was not true of the thinner joints, where the total extension of the gage length was usually less than 2 percent.

A.3. Discussion of Current and Thickness Effects

Overall, the dominant factor in bond strength was the thickness. Only a small joint thickness window was available (35 μm to 70 μm) where a sound joint was consistently achieved. In this thickness range, the bond strength was in the range of the ultimate strength of the copper substrate. Above this thickness, a triaxial stress state was

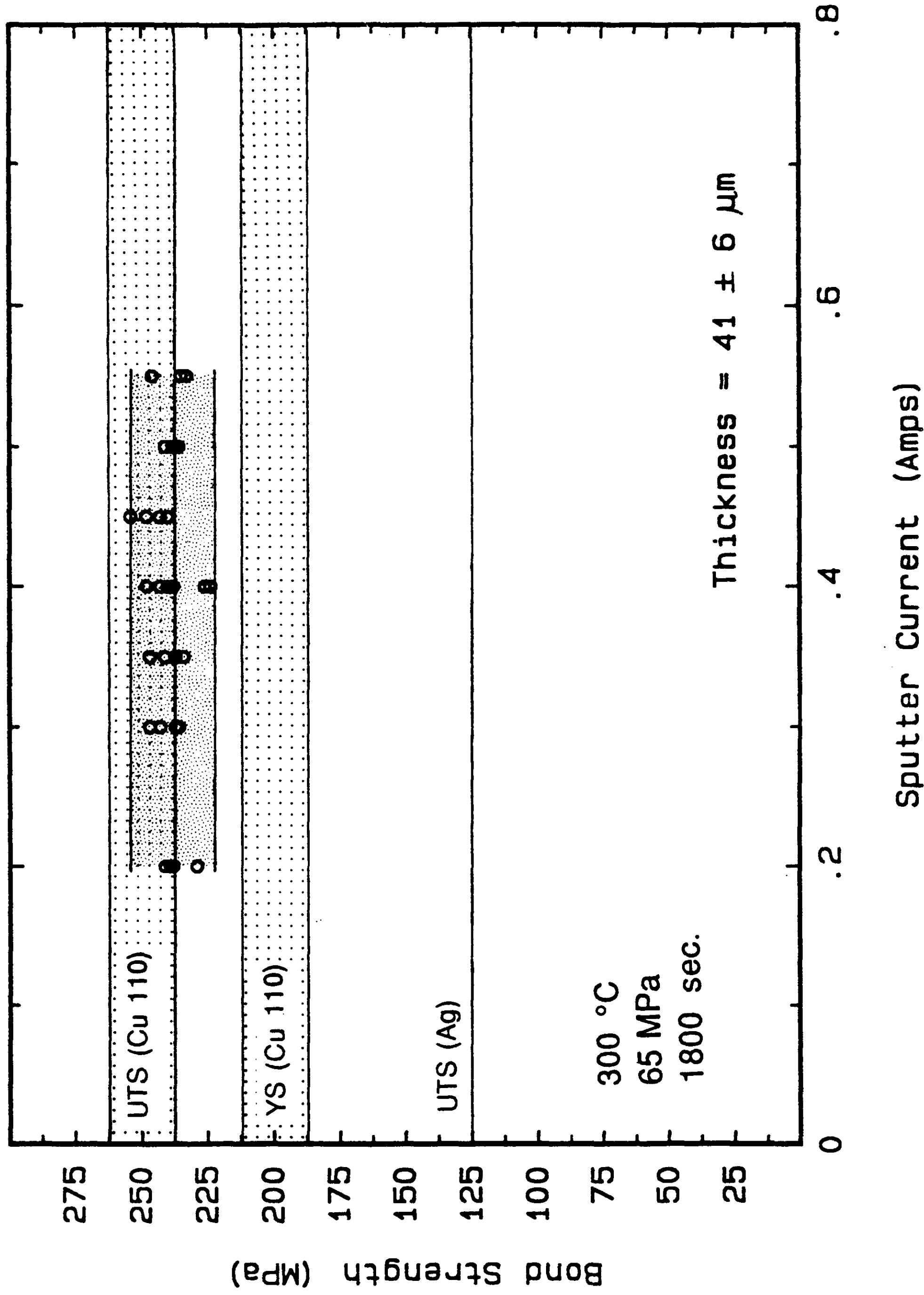

Figure 3.7: Bond strength versus sputter deposition current for a joint thickness of 41 ± 6 μm.

not achieved. Below this thickness, the prior copper surface roughness began to hinder plastic deformation and data irreproducibility became a problem. It is only for these thin joints that the deposition current affected the bond strength. A simple relationship between bond strength and deposition sputter current was not apparent.

A.4. Effect of Bonding Pressure and Temperature

An effort was also made to achieve a full strength bond at temperatures below 300 °C. As the temperature was decreased, the bonding pressure was increased in an attempt to compensate for the increase in the flow stress of the silver at lower temperatures. The best coating conditions from the 300 °C test matrix were used. The sputter current was 0.40 amperes and the joint thickness was approximately 40 µm. The results of these tests are shown in Figure 3.8. At 220 °C (medium T), a relatively high bond strength (200 MPa) was obtained when the applied bonding pressure was between 100 and 125 MPa. When the temperature was lowered to 150 °C (low T), the maximum bond strength was only 50 MPa, even for an applied pressure of 165 MPa. A bond strength of only a few MPa was achieved at 100 °C (low T) with an applied stress of 150 MPa. This agrees with the work of Munir [9], and Mohamed and Washburn [4] who predicted a large drop in bond strength below 190 °C due to the thermal stability of silver oxide below this temperature.

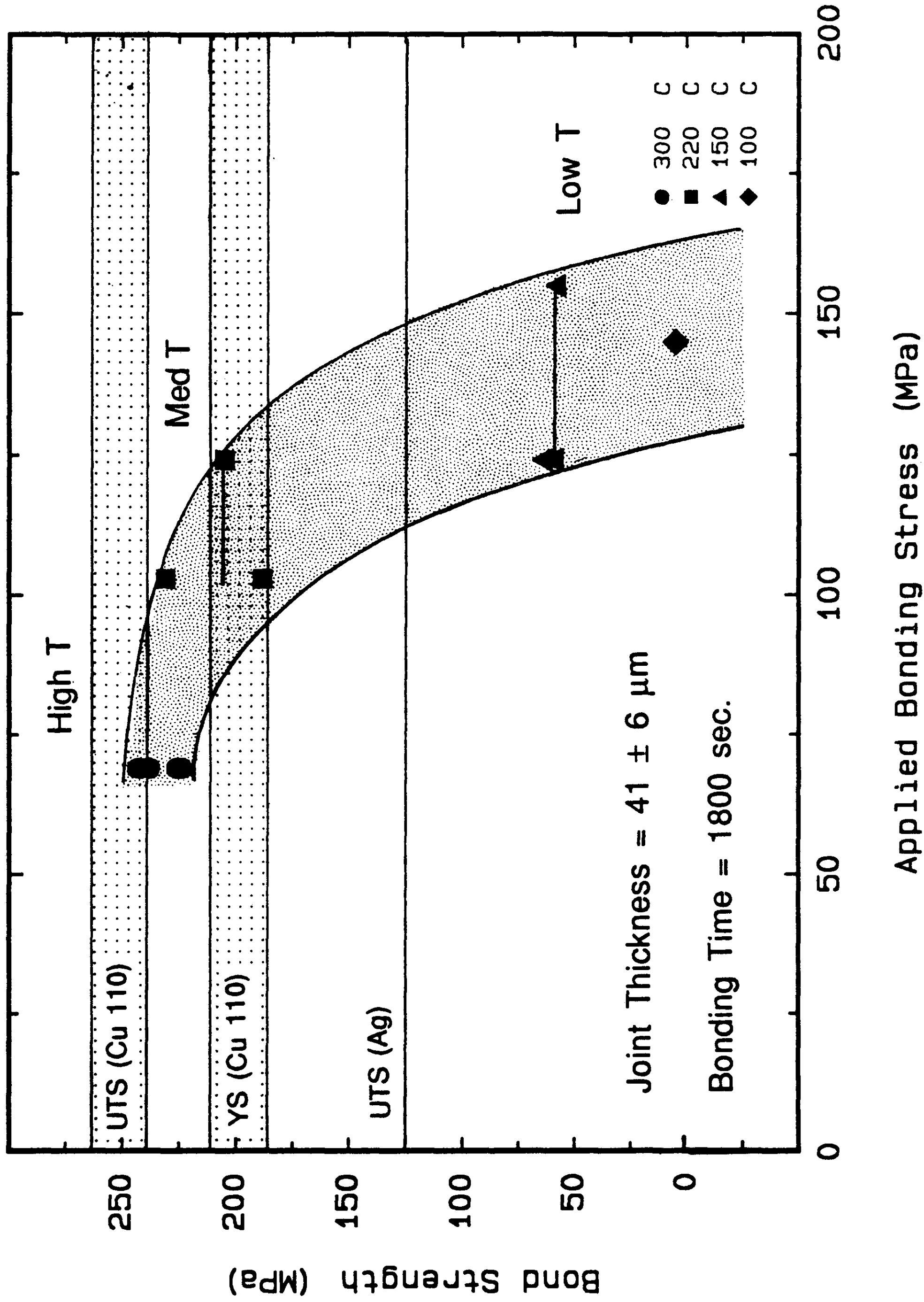

Figure 3.8: Bond strength as a function of bonding pressure for several temperatures.

B. Crystallographic Orientation of Sputtered Coatings

The as-machined copper surfaces had a {200} preferred orientation. All of the coatings except the 1-μm-thick coating showed some degree of preferred orientation. The coatings always had either a {111} or {220} preferred orientation parallel to the coated surface. The relative degree of preferred orientation was calculated by dividing the height of the second highest intensity peak by the height of the highest intensity peak (I{111}/I{220} or I{220}/I{111}) so that the degree of preferred orientation is reported as a fraction between +1 and -1. A positive fraction is a {220} preferred orientation and a negative fraction is a {111} orientation. The bond strength was found to independent of the preferred orientation except for the relatively thin (12-μm-thick) joints.

B.1. Crystallographic Orientation of As-machined Copper Surfaces

X-ray diffraction measurements were done on three as-machined copper samples and on two samples with thin (< 2-μm-thick) silver coatings. The results are summarized in Table 3.1 along with the relative peak intensities measured from a randomly oriented powder sample. All of the samples had a preferred {200} orientation parallel to the machined surface. The intensity of the {200} peaks relative to the {111} peaks were 11 to 276 percent higher than the peaks for a randomly oriented powder. In addition, both the {220} and {311} peak intensities decreased relative to the {111} peaks.

Table 3.1: Relative peak intensities for as-machined copper samples.

Sample Number	I{111}	I{200}	I{220}	I{311}	% Change I{200}/I{111}
1	1.00	0.51	0.02	0.10	+ 11
2	1.00	1.73	<0.01	0.05	+276
3	1.00	0.73	0.03	0.08	+ 59
4	1.00	1.22	0.03	0.15	+165
5	1.00	0.89	0.02	0.07	+ 93
randomly oriented powder*	1.00	0.46	0.20	0.17	--

*Source: ICPDS Data Book, Vol. 1, p. 89.

B.2. Effect of Thickness on Orientation

In the coating thickness range of 6 μm to 21 μm, similar trends in change in orientation as a function of thickness were observed for the 0.20-ampere, the 0.40-ampere and the 0.55-ampere sputter deposition currents. The orientation as a function of thickness is shown in Figure 3.9. For the 0.20-ampere coating, the crystallographic orientation parallel to the surface was strongly {220} at a coating thickness of 6 μm. When the coating thickness was increased to 12 μm, the orientation changed to a strong {111}

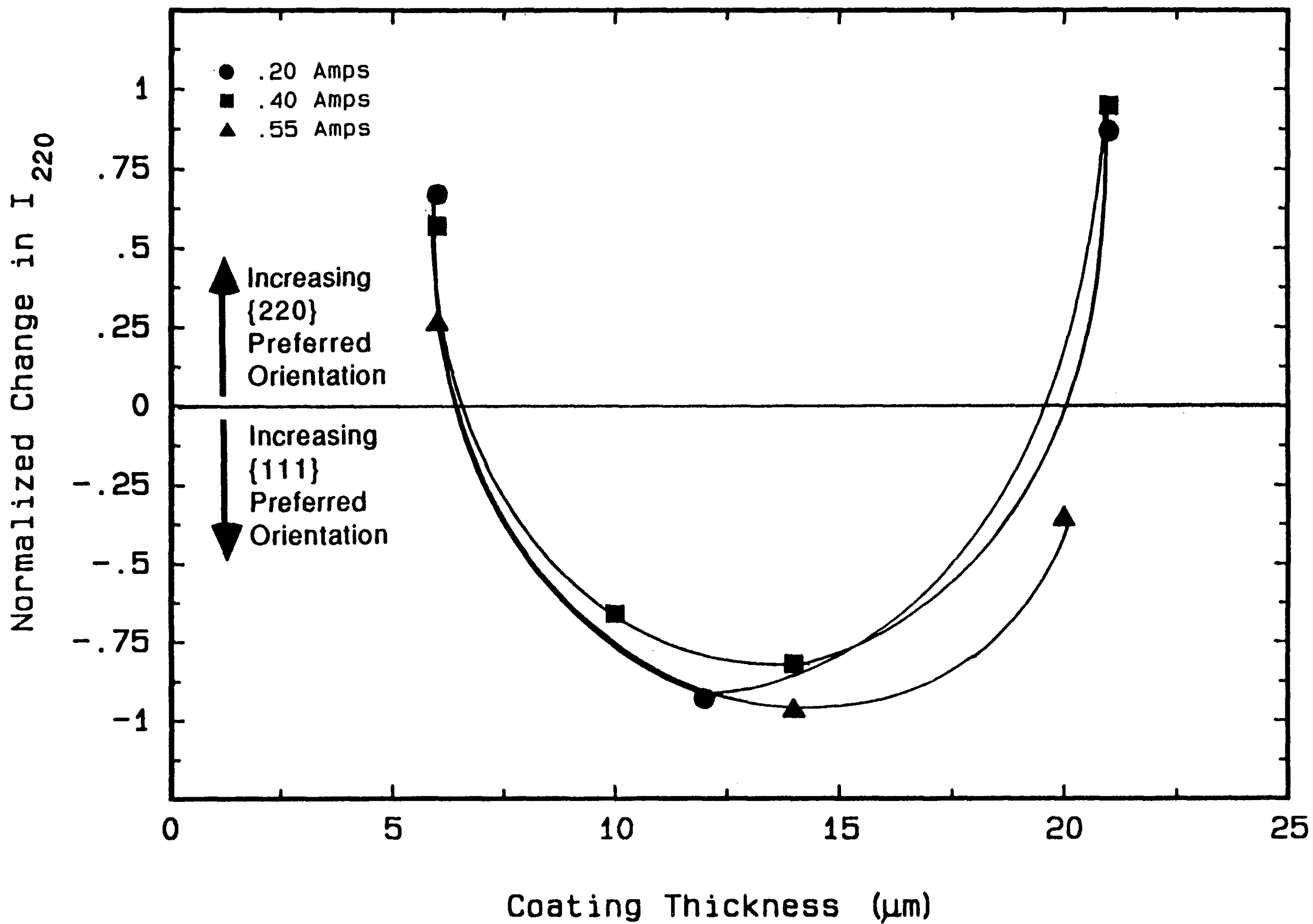

Figure 3.9: Combined plot of preferred orientation versus thickness for 0.20, 0.40 and 0.55 amp sputter deposition currents.

orientation. At a coating thickness of 20 μm, the orientation shifted back to a {220} orientation.

A similar trend in preferred orientation was observed for the 0.40-ampere coatings. In the thickness range of 6 μm to 25 μm, the crystallographic orientation again shifted from strongly preferred {220} orientation to strongly preferred {111} orientation and back to a strongly preferred {220} orientation with increasing thickness.

The 0.55 ampere coating also started with a {220} preferred orientation at a thickness of 6 μm and the orientation again changed to a strong {111} orientation as the coating thickness was increased to 14 μm. However, at a coating thickness of 20 μm, the crystallographic orientation did not shift back to a strong {220} but instead it changed to a slightly preferred {111} orientation.

The thickness range was extended for the 0.40-ampere coatings and is shown in Figure 3.10. There was no preferred orientation for the 1-μm-thick coating. The 2-μm-thick and 6-μm-thick coatings had a {220} orientation. A shift to a {111} preferred orientation was observed from 10 to 15 μm. At 20 μm, the preferred orientation shifted back to a {220} orientation and remained {220} up to 43 μm which was the thickest coating produced in this study.

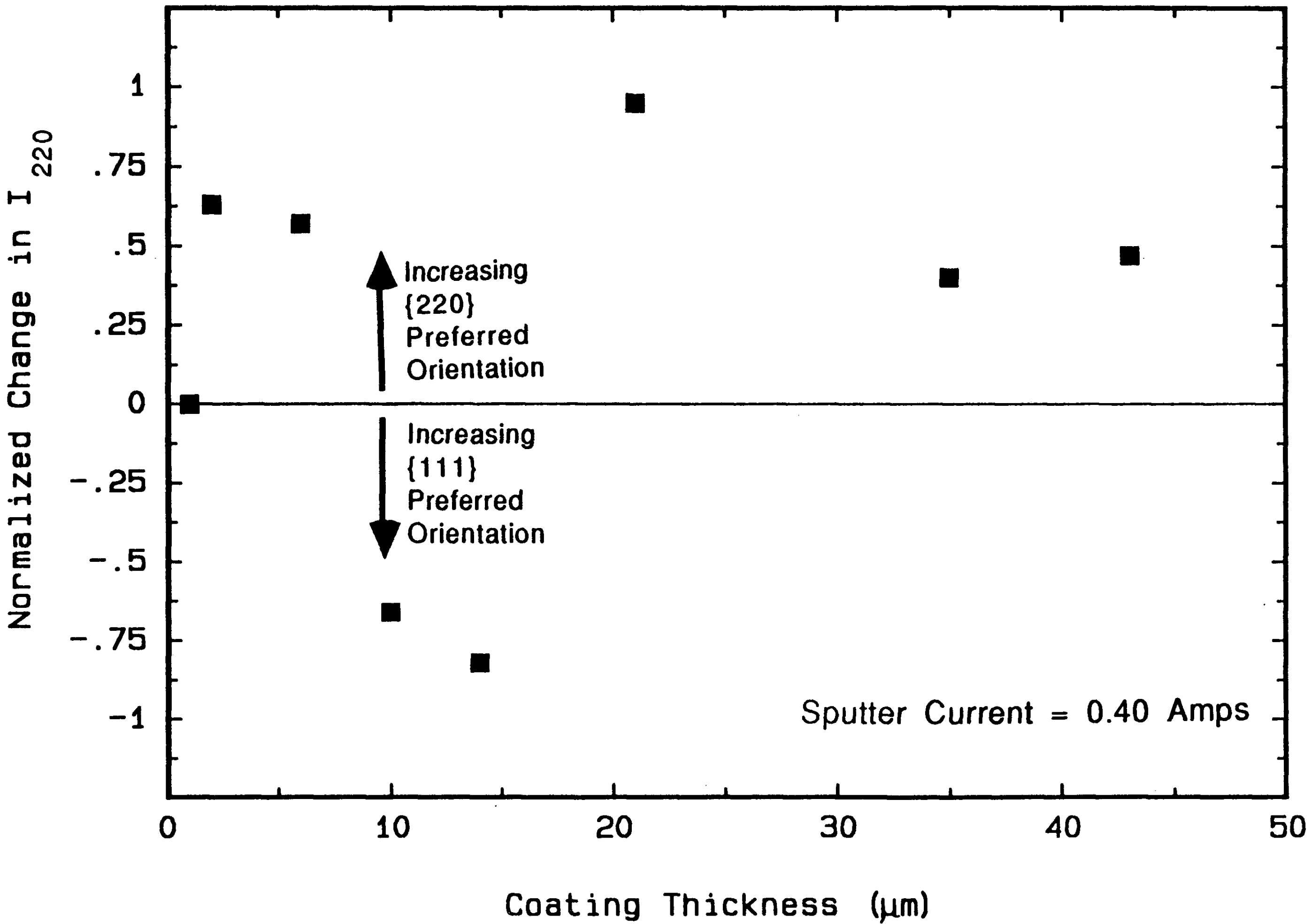

Figure 3.10: Preferred orientation versus thickness for a 0.40 amp sputter deposition current over the extended thickness range of 1 µm to 43 µm.

ARTHUR LAKES LIBRARY
COLORADO SCHOOL of MINES
GOLDEN, COLORADO 80401

B.3. Effect of Sputter Current on Orientation

While the constant current data showed trends in preferred orientation development, there were large variations in the constant thickness data, especially for the 6-μm-thick coatings. This may be partially due to the difficulty in maintaining a constant deposition current at the current extremes (0.10 and 0.70 amperes). Figure 3.11 shows the change in preferred orientation with sputter current at a coating thickness of 6 ± 1 μm. In the current range of 0.20 amperes to 0.55 amperes, a trend of decreasing {220} orientation with increasing current was observed. However, in the full current range of 0.10 to 0.70 amperes, there were no definite trends.

At a coating thickness of 13 ± 2 μm, all of the coatings except the 0.10-ampere sputtered coating had a strongly preferred {111} orientation. The 0.10-ampere coating had a slight {220} preferred orientation. These data are plotted in Figure 3.12.

Figure 3.13 shows the change in preferred orientation versus current for a coating thickness of 20 ± 3 μm. At this thickness, there was a definite trend in the orientation as a function of sputter current. When the current was less than or equal to 0.40 amperes, there is a strong {220} orientation. There appears to be a critical current of between 0.40 and 0.45 amperes, above which the preferred growth orientation switched to slightly {111}.

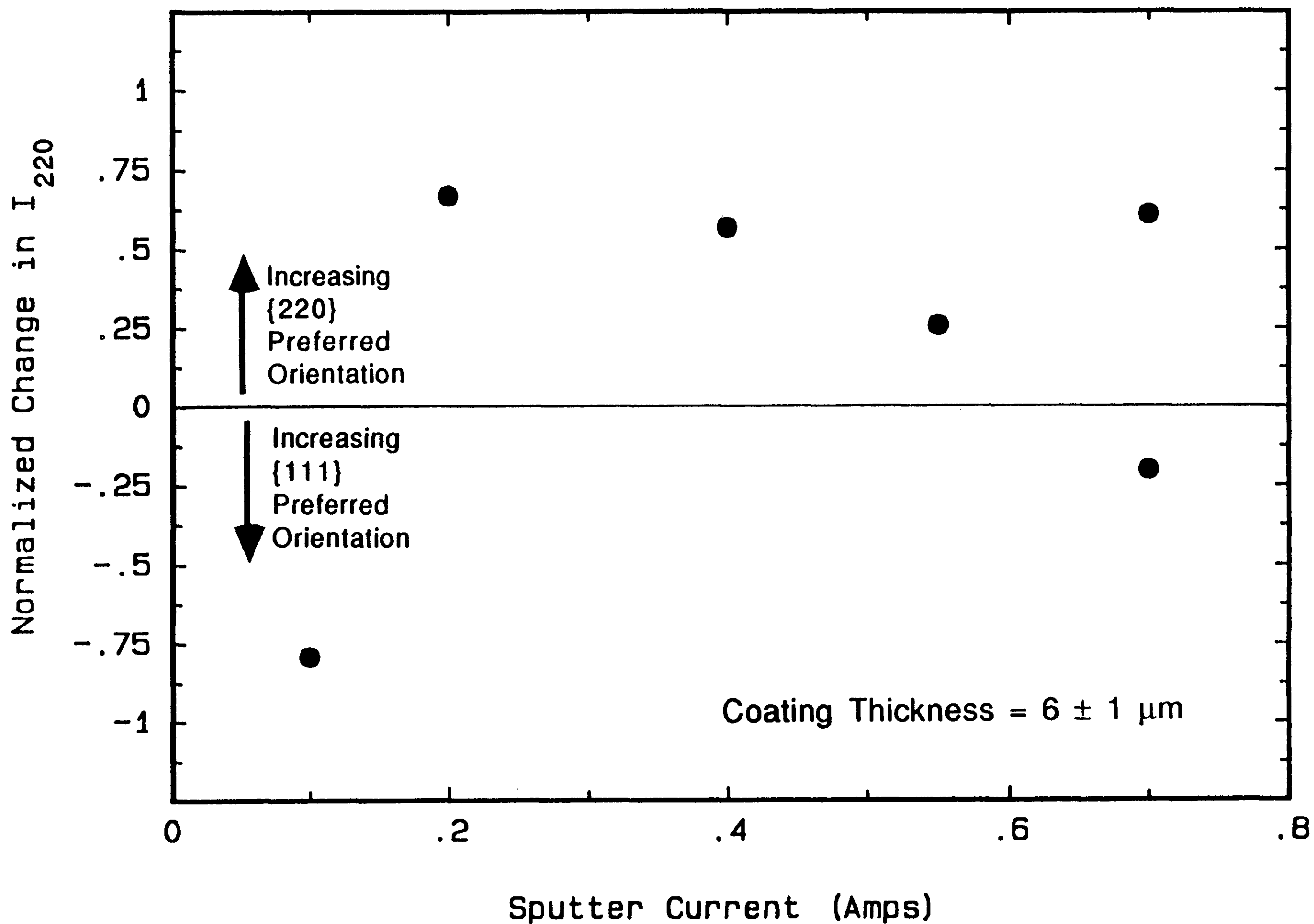

Figure 3.11: Preferred orientation versus sputter deposition current for a coating thickness of 6 ± 1 μm.

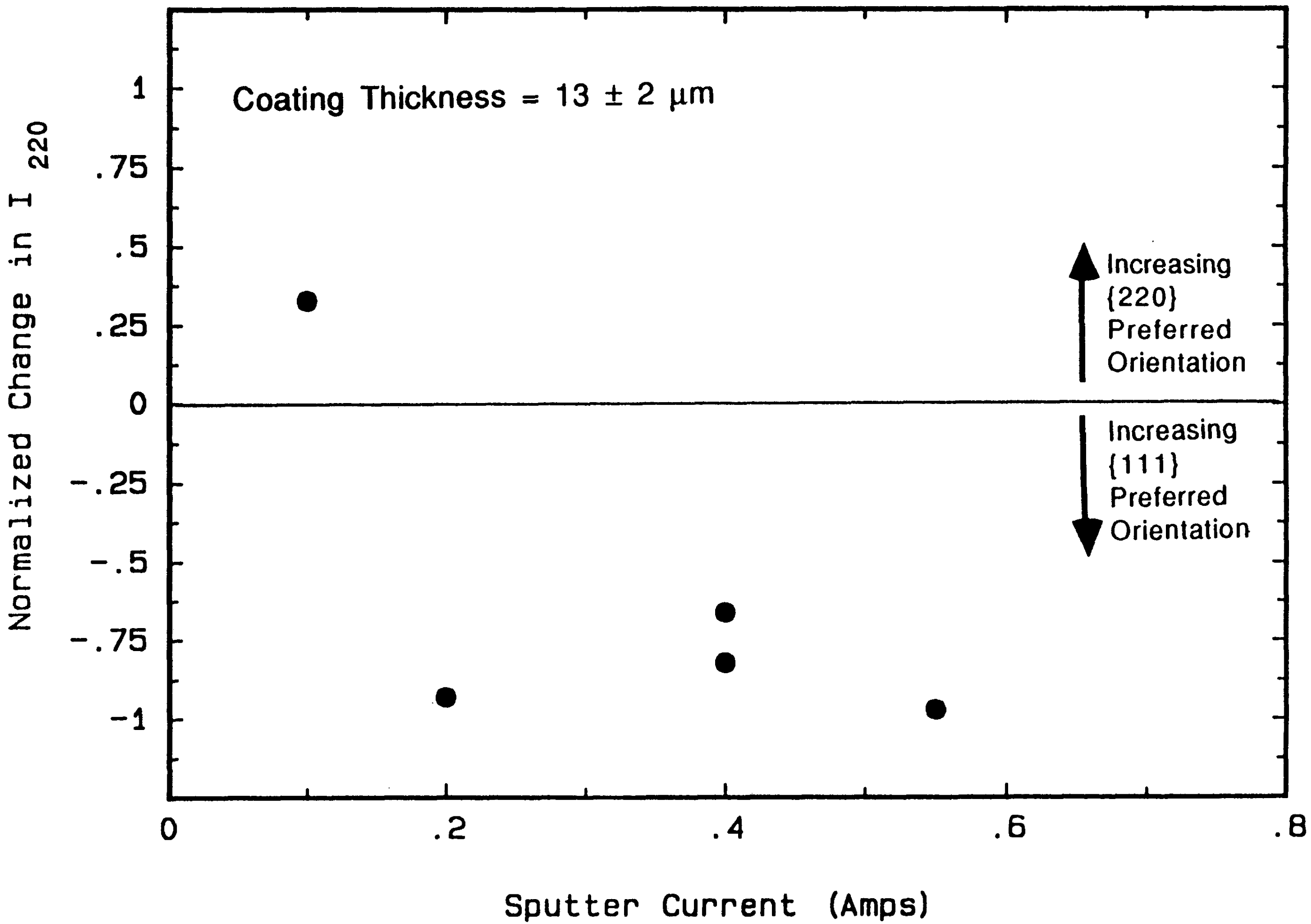

Figure 3.12: Preferred orientation versus sputter deposition current for a coating thickness of 13 ± 2 μm.

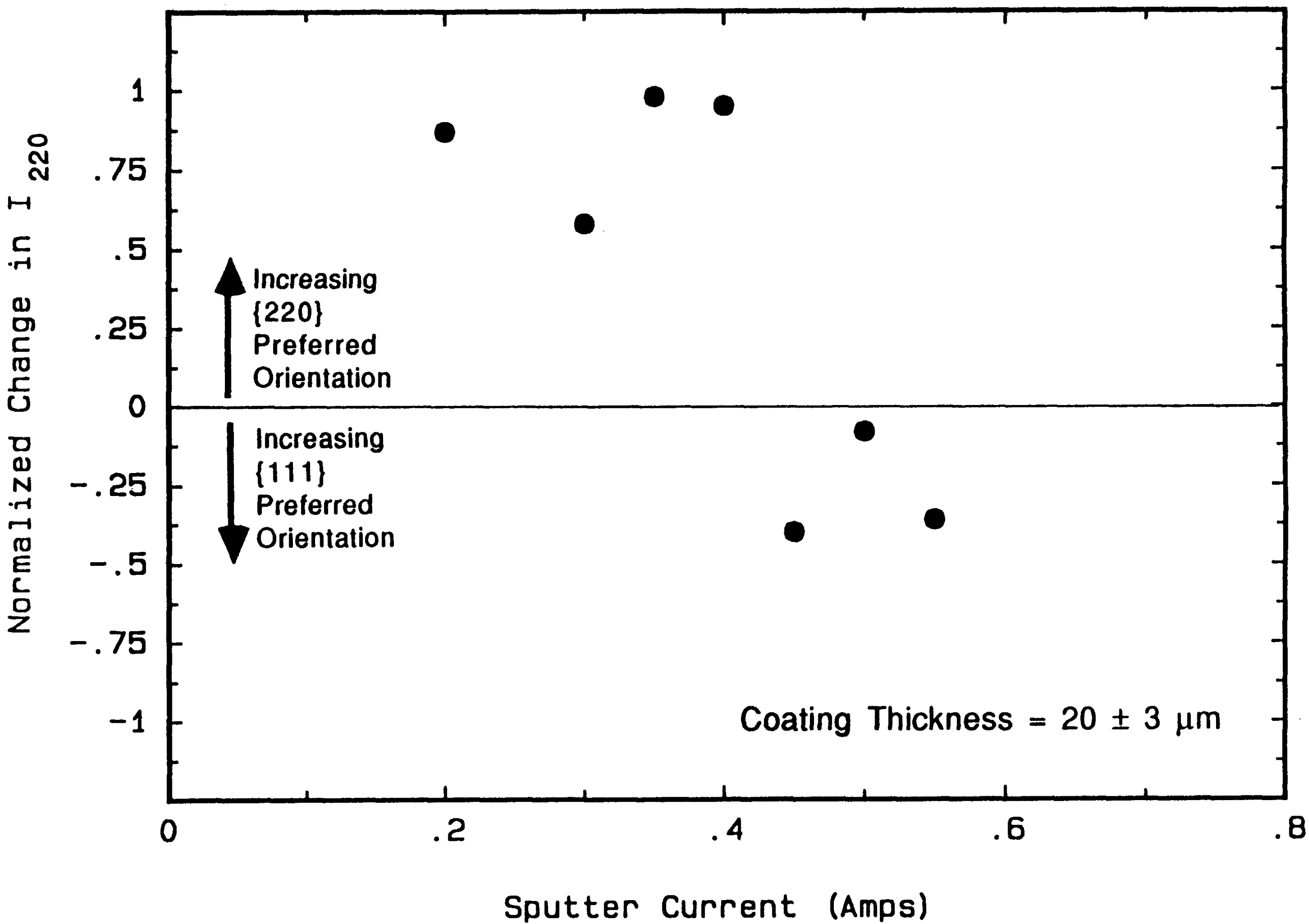

Figure 3.13: Preferred orientation versus sputter deposition current for a coating thickness of 20 ± 3 μm.

B.4. Effect of Preferred Orientation on Bond Strength

Figure 3.14 shows the average bond strength for a given coating condition versus its degree of preferred for a joint thickness of 12 ± 2 µm. Each data point represents the average bond strength of from two to four bonds made with samples from the same coating run. The bond strength increases as the coating orientation changes from a highly preferred {111} orientation to a highly preferred {220} orientation. For a strong {111} orientation, the average bond strength was only 93 MPa, while for a strong {220} orientation the average bond strength was 230 MPa. The 0.10-ampere coating run resulted in the lowest average bond strength (93 MPa). The lower bond strengths may have been the result of surface oxidation during sputter coating. The surface morphology suggested that silver oxide particles may have contaminated the surface. This will be discussed in greater detail in the Microstructure section. The oxidation appears to have been minimal as it did not show up in the x-ray diffraction data. The data points from two other coating runs were discarded when silver oxide peaks showed up in their x-ray diffraction profiles. Even if the data point from the 0.10-ampere coating was eliminated, the bond strength still increased from 160 MPa to 230 MPa as the orientation changed from a {111} orientation to a {220} orientation.

For joint thicknesses of 26 ± 4 µm and 41 ± 6 µm, this same behavior was not observed. The bond strength versus preferred orientation for these thicknesses is shown in Figures 3.15 and 3.16

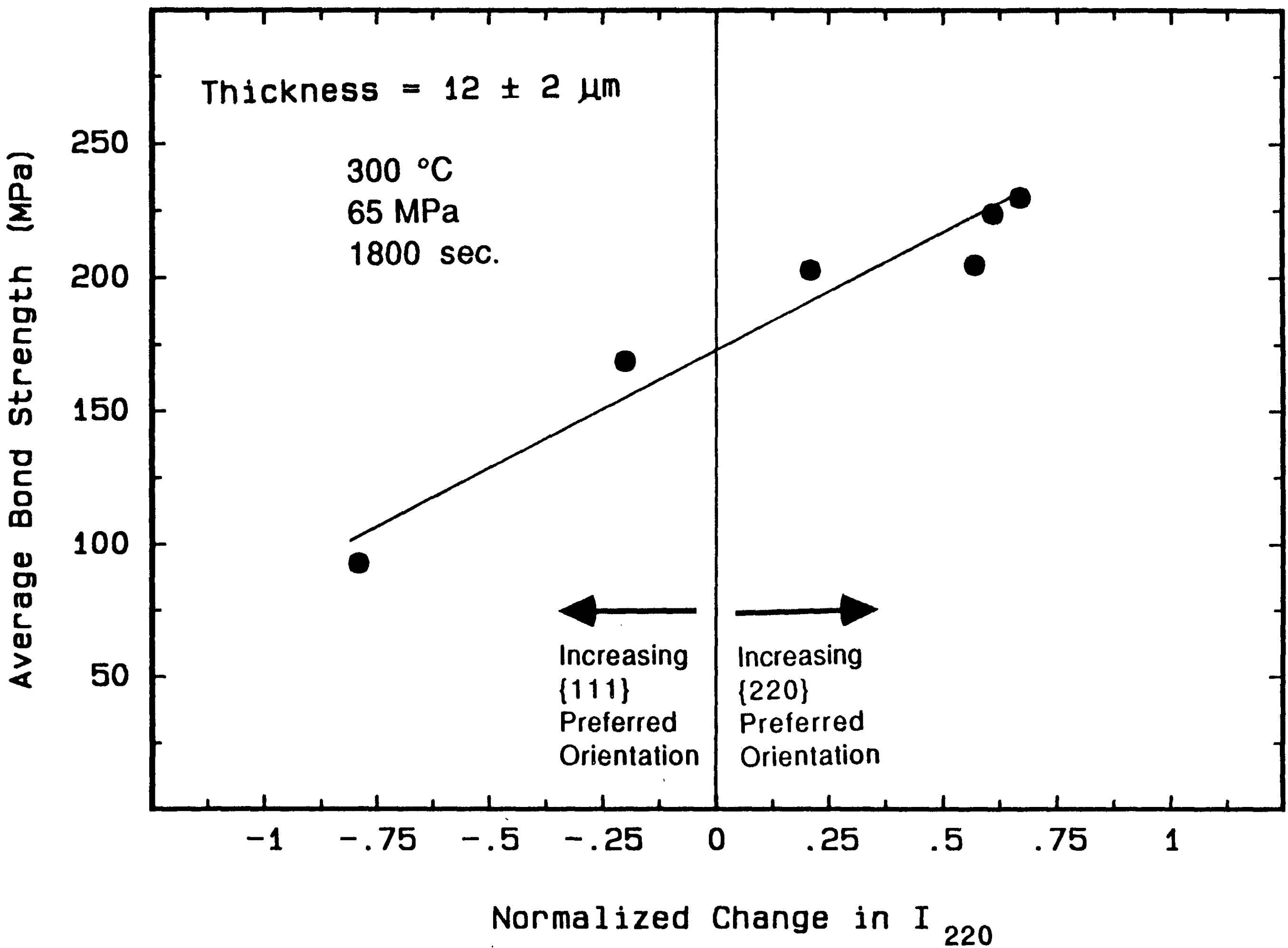

Figure 3.14: Average bond strength versus degree of preferred orientation for a joint thickness of 12 ± 2 µm.

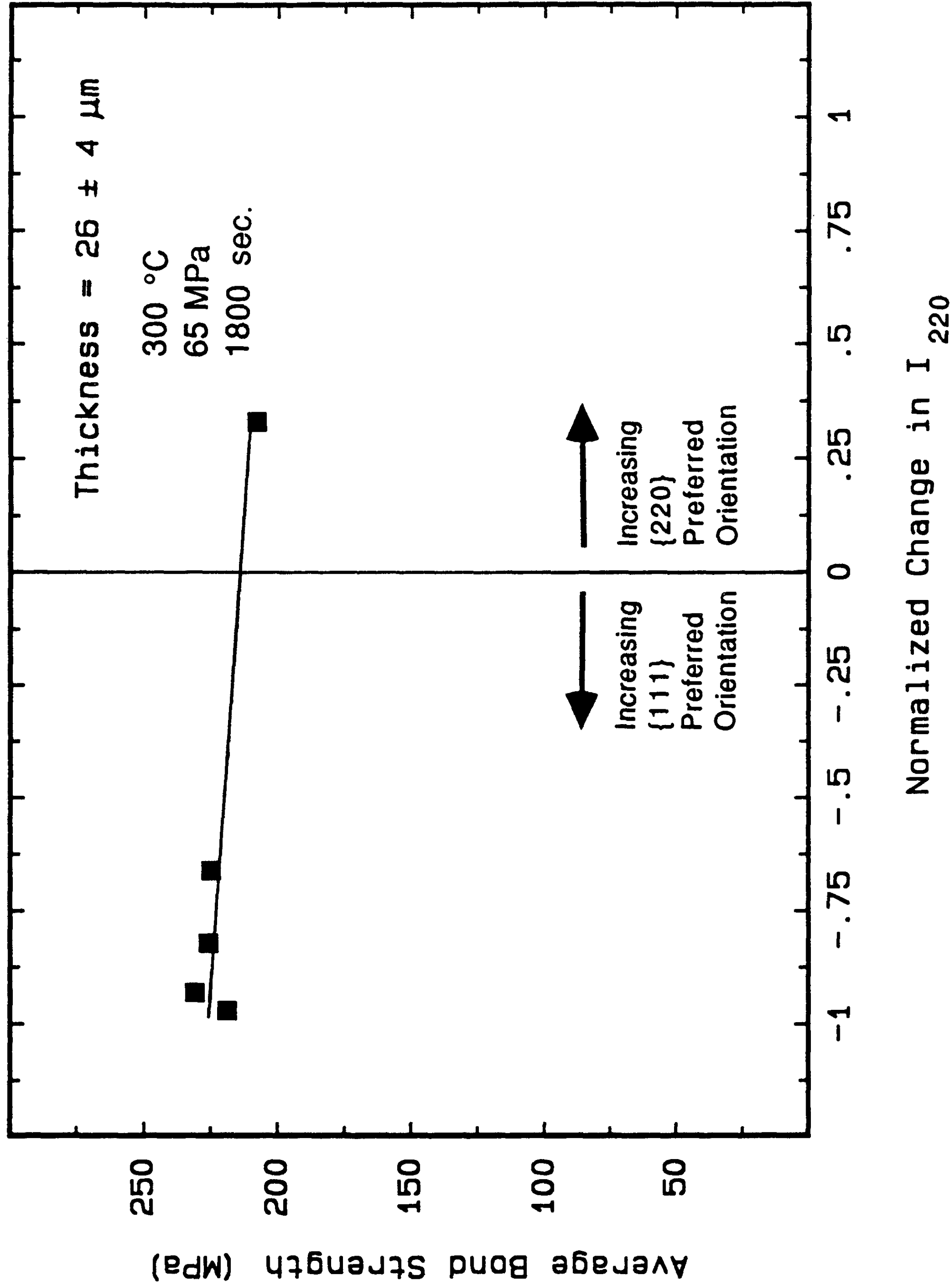

Figure 3.15: Average bond strength versus degree of preferred orientation for a joint thickness of 26 ± 4 μm.

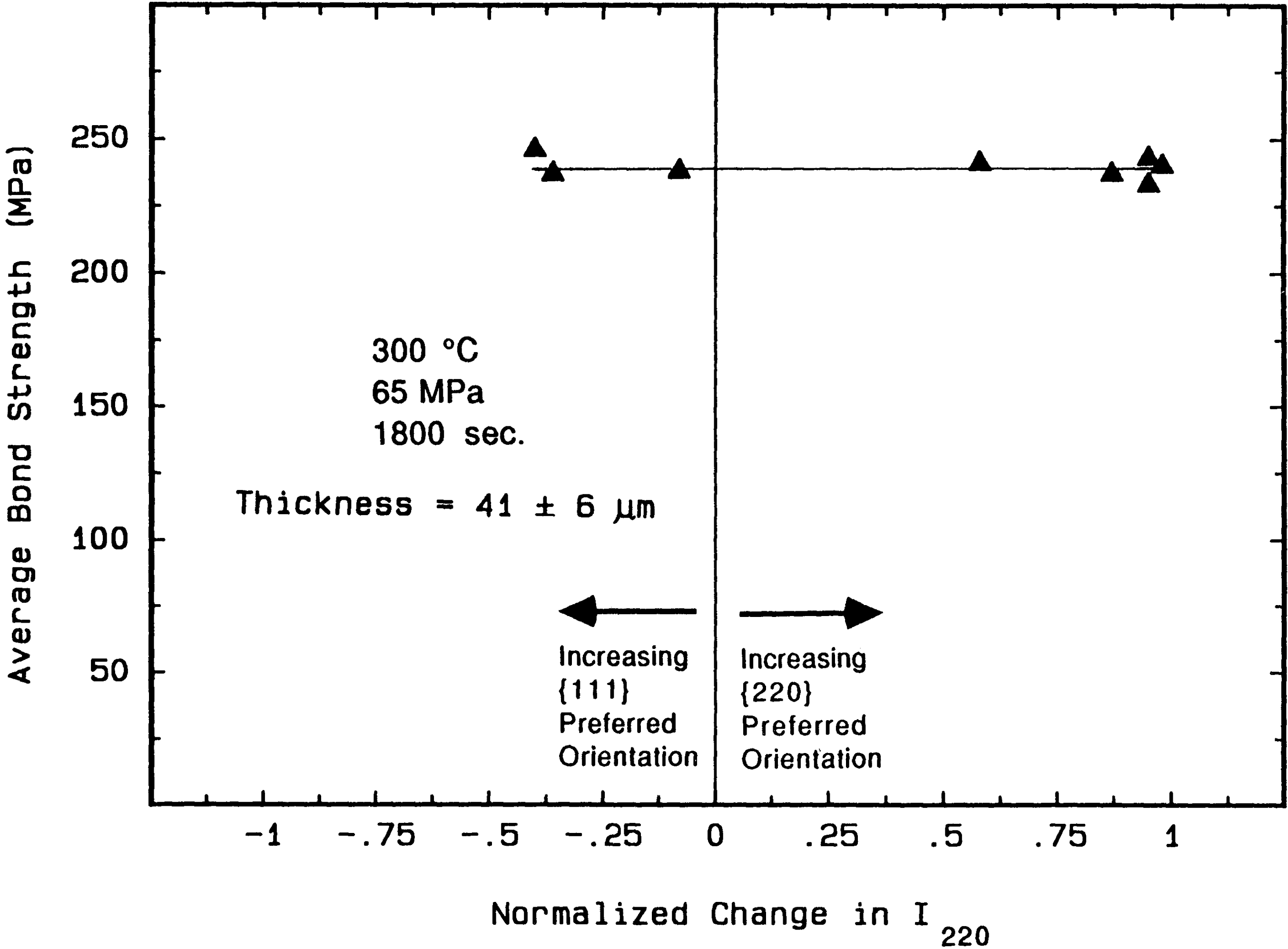

Figure 3.16: Average bond strength versus degree of preferred orientation for a joint thickness of 41 ± 6μm.

respectively. For both of these conditions, the bond strength is relatively constant for a wide range of {220} and {111} preferred orientations.

B.5. Discussion of Preferred Orientation Effects

When silver was coated on copper which had a {200} preferred orientation parallel to its machined surface, both {111} and {220} preferred coating orientations were observed. In the current range 0.20 amperes to 0.55 amperes and thickness range 6 μm to 43 μm, it was possible to predict which preferred would be present. However it was not possible to predict the degree of preferred orientation. This may be due to the variation in the degree of preferred orientation of the copper substrate which could alter the initial growth pattern. Outside of the 0.20 to 0.55 ampere current range, it became difficult to maintain a constant current which made it impossible to predict which orientation would be preferred.

For the thick joints (26 and 41 μm), the joint strength was relatively constant for a wide range of {111} and {220} preferred orientations. However, at a joint thickness of 12 μm the preferred orientation was a major factor in determining the bond strength. At this joint thickness, the bond strength increased from approximately 90 MPa to 230 MPa as the orientation was changed from a highly preferred {111} orientation to a highly preferred {220} orientation. At this thickness, the surface roughness may be hindering the coatings

ability to plastically deform such that only the {220} orientation deforms enough to give good contact. Since silver is face-centered cubic, twelve different slip systems can operate in a single crystal. Crystallographic orientation is a major factor in determining which slip systems will operate. For a single crystal with a (220) orientation perpendicular to an applied uniaxial stress, four slip systems operate with a Schmid factor ($\cos\theta \cos\phi$) of 0.408. For the same single crystal with a (111) orientation perpendicular to the applied stress, six slip systems operate but their Schmid factor is now 0.384. The slip systems which operate are summarized in Table 3.2 for the (220) and (111) orientations. Slip will occur when the applied stress causes the shear stress (τ) to be greater than the critical resolved shear stress (τ_{CRSS}):

$$\tau_{CRSS} \leq \tau = \sigma \cos\phi \cos\theta \quad (1)$$

where σ = applied uniaxial stress
θ = angle between slip plane normal and stress axis
ϕ = angle between slip direction and stress axis

Rearranging equation (1) to solve for the applied uniaxial stress necessary to cause slip:

$$\sigma = \tau_{CRSS} / (\cos\phi \cos\theta) \quad (2)$$

Using this analysis with a critical resolved shear stress of 350 kPa for silver [31], an applied tensile stress of 850 kPa is needed to cause

Table 3.2: Schmid factors for slip systems in a silver single crystal with (111) and (220) planes oriented perpendicular to an applied uniaxial stress.

Slip System	Schmid Factor	
	(220)	(111)
$(111)\langle\bar{1}10\rangle$	0	0
$(111)\langle 10\bar{1}\rangle$	0.408	0
$(111)\langle 01\bar{1}\rangle$	0.408	0
$(1\bar{1}1)\langle 011\rangle$	0	0.384
$(1\bar{1}1)\langle 10\bar{1}\rangle$	0	0
$(1\bar{1}1)\langle 110\rangle$	0	0.384
$(11\bar{1})\langle 011\rangle$	0.408	0.384
$(11\bar{1})\langle 101\rangle$	0.408	0.384
$(11\bar{1})\langle\bar{1}10\rangle$	0	0
$(\bar{1}11)\langle 01\bar{1}\rangle$	0	0
$(\bar{1}11)\langle 101\rangle$	0	0.384
$(\bar{1}11)\langle 110\rangle$	0	0.384

slip in a single crystal with a (220) orientation while an applied stress of 1300 kPa is needed for slip with a (111) orientation. If a constant grain size is assumed, it will be easier to plastically deform a coating with a (220) orientation.

C. Microstructure

The sputtered silver coatings had a wide variety of surface morphologies which varied with both thickness and coating deposition current. The surface had a very fine microstructure which could be observed using an SEM. No surface etching was necessary. The machining lines on the copper surfaces were still visible even for thick coatings. No correlation was found between the surface morphology and the bond strength or preferred orientation.

C.1. As-machined Copper Surfaces

The as-machined copper samples had a very regular surface consisting of parallel machining ridges. A typical surface is shown at magnifications of 200X and 2000X in Figure 3.17. All of the samples had a very similar appearance. Most of the bonding surface was very regular but they all had isolated regions of microtearing. Figure 3.18 shows a typical microtear which is less than 10 μm long and 5 μm wide. These microtears may be due to inclusions in the metal.

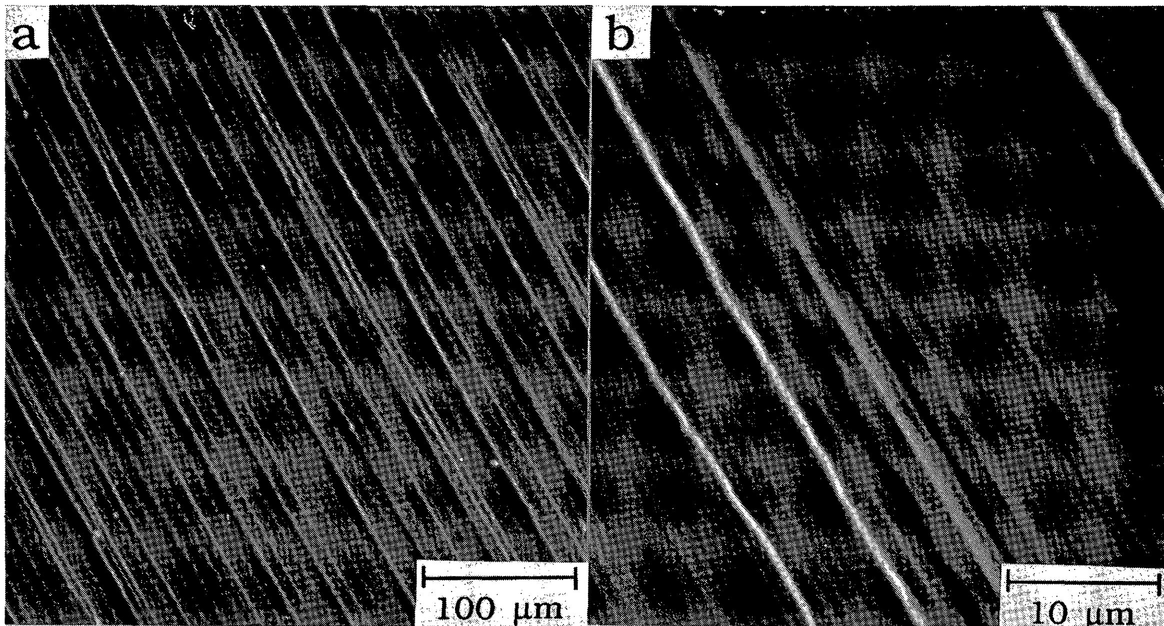

Figure 3.17: SEM photographs of as-machined copper substrate a.) 200X b.) 2000X.

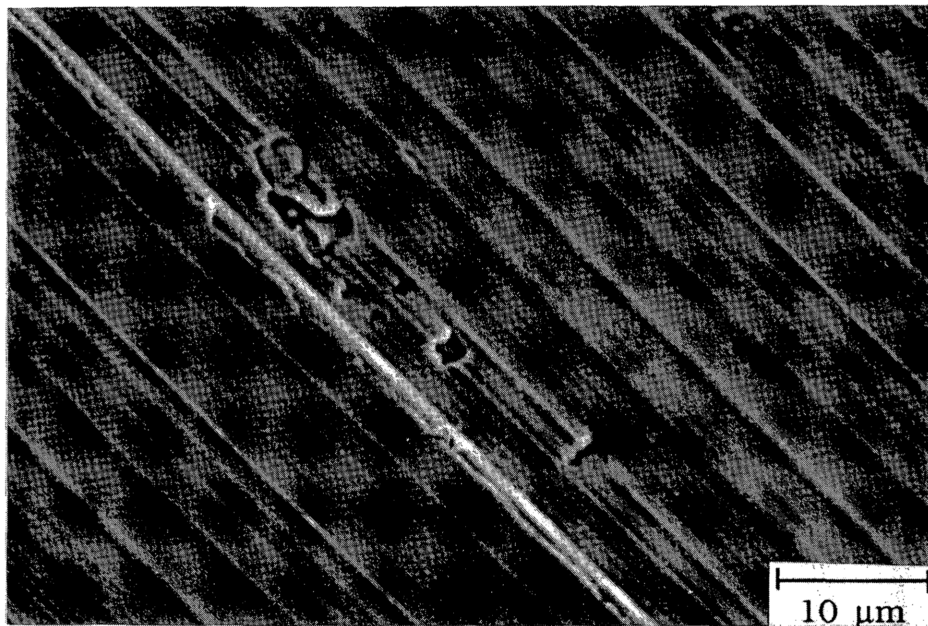

Figure 3.18: SEM photograph of as-machined copper substrate showing microtearing (2000X).

C.2. Coating Morphology

At low magnifications (200X), all of the coatings had a very similar appearance. Regardless of the thickness, the machining lines were still visible. In most cases, the surface had a roughened appearance because of holes and domes which formed on the surface. The as-coated surfaces are shown for several coating conditions in Figure 3.19. The machining lines were still visible even for the 43-μm-thick coating.

At higher magnifications (5000X), the domes appeared to be different growth modes. The 6-μm-thick coatings all had at least one common growth mode consisting of very fine grains which are less than 0.1 μm in diameter. Since the coatings had a very strong preferred orientation, these are probably the tops of long cylindrical columnar grains. With the exception of the 0.40 ampere coating, this is the dominant surface feature. In addition, all of the coatings exhibited at least one other growth mode. Two coating runs were done at a sputter current of 0.70 amperes and even these samples had different coating morphologies. The sample from the first 0.70-ampere coating run had several randomly spaced domes on its surface. They ranged in size from 1 μm to greater than 10 μm in diameter. This was the most common coating morphology. The 0.20-ampere and the 0.55-ampere coatings had very similar appearances. For the 0.10-ampere and 0.40-ampere coatings, the large domes were still present but most had a diameter of less than 5 μm. However these

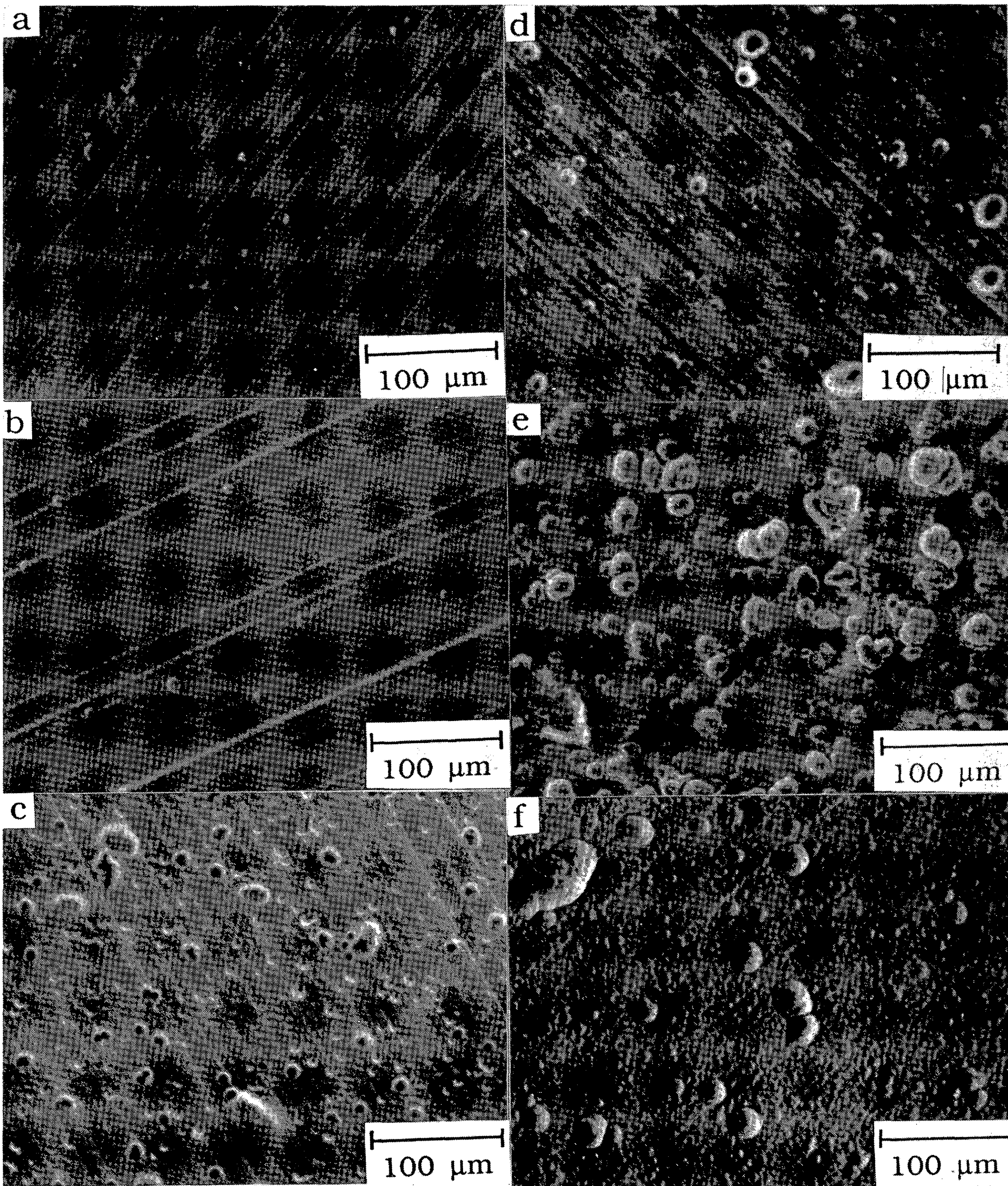

Figure 3.19: Low magnification (200X) SEM photographs of as-coated sample surfaces showing roughened surface and machining lines: a.) 1 μm, 0.40 amps b.) 13 μm, 0.40 amps c.) 13 μm, 0.20 amps d.) 20 μm, 0.40 amps e.) 20 μm, 0.45 amps f.) 43 μm, 0.40 amps.

coatings exhibited a third growth mode which consisted of many smaller domes which were approximately 0.5 μm to 2 μm in diameter. For the 0.40-ampere coating, the small domes were the dominant surface feature. The 0.70-ampere sample from the second coating run was very similar to the first 0.70-ampere coated sample except that a large number of the domes are elongated and follow the machining ridges. This anomolous behavior may be due to a misalignment between the silver target and the copper substrate during sputtering. A misalignment could cause one side of the ridge to be shielded from the incoming sputtered atoms by the other side of the ridge. It could also be due to improper machining leading to the wrong surface roughness. Since one of the goals of this experiment was to examine the effect of coating microstructure on bond strength, the microstructure from this coating run was studied even though its reproducibility was questionable.

Even though a wide variety of coating morphologies were produced at this thickness, no correlation was found between surface morphology and bond strength (or preferred orientation). Figure 3.20 shows high magnification (5000X) SEM photographs of each of the different surface morphologies. They are arranged from lowest bond strength to highest bond strength. This also corresponds to a shift from a strong {111} orientation to a strong {220} orientation. The surface which resulted in the lowest average bond strength had shiny particles on it which may have been oxide particles. All of the other

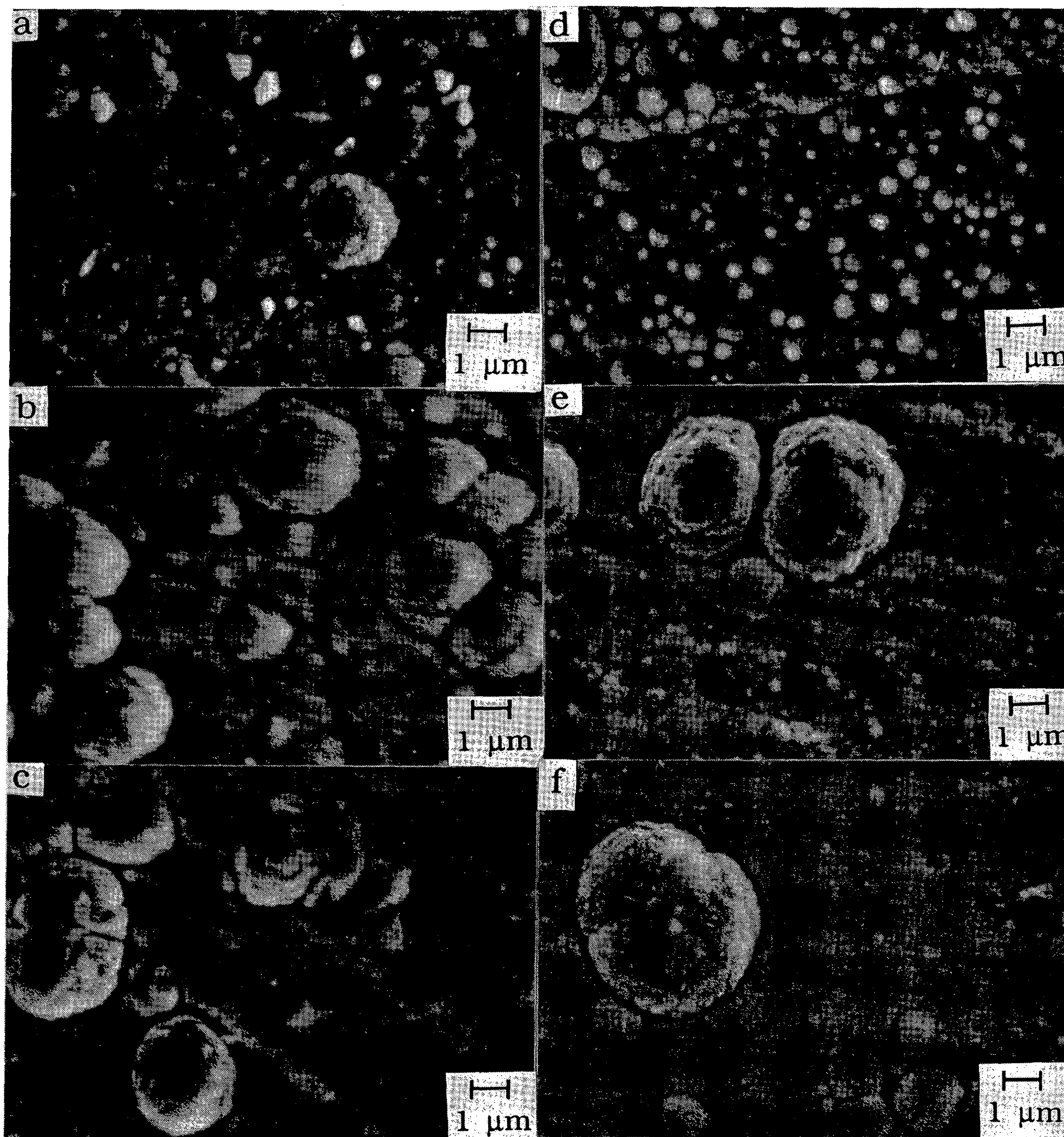

Figure 3.20: SEM photographs of surfaces of as-coated 6 ± 1-µm-thick sputtered silver coatings (5000X). The samples are arranged from the lowest bond strength to the highest bond strength (from the strongest {111} orientation to the strongest {220} orientation): a.) 0.10 amps b.) 0.70 amps (1st coating run) c.) 0.55 amps d.) 0.40 amps e.) 0.70 amps (2nd coating run) f.) 00.20 amps.

ARTHUR LAKES LIBRARY
COLORADO SCHOOL of MINES
GOLDEN, COLORADO 80401

coating morphologies were randomly distributed at different bond strengths and preferred orientations.

The 13-μm-thick coatings also had a wide variety of coating morphologies. At this thickness, the sputter current ranged from 0.10 to 0.55 amperes. Two coating runs were done at 0.40 amperes to check for data reproducibility. Both of the 0.40-ampere samples and the 0.55-ampere sample had the same bimodal growth modes observed on most of the thinner coatings. This was several large domes (1 μm to greater than 10 μm in diameter) surrounded by very fine grains (less than 0.1 μm in diameter). The other two samples had very different morphologies. The 0.20-ampere coating also consisted of very fine grains and large domes. However, all of the surface including the domes had an blocky, angular appearance. The 0.10 ampere coating had only a single growth mode. It consisted of equiaxed grains with an average grain diameter of 1.33 μm which was calculated using the line-intercept method. SEM photographs of the 13-μm-thick coatings are shown in Figure 3.21. The surfaces are arranged from the strongest {111} orientation to the strongest {220} orientation. There was no apparent correlation between the coating morphology and orientation. The bond strength was approximately constant even though a wide variety of morphologies were observed.

The 20-μm-thick coatings were very similar to the 13-μm coatings except relatively large equiaxed grains were formed on some of the surfaces. The sputter current ranged from 0.20 to 0.55

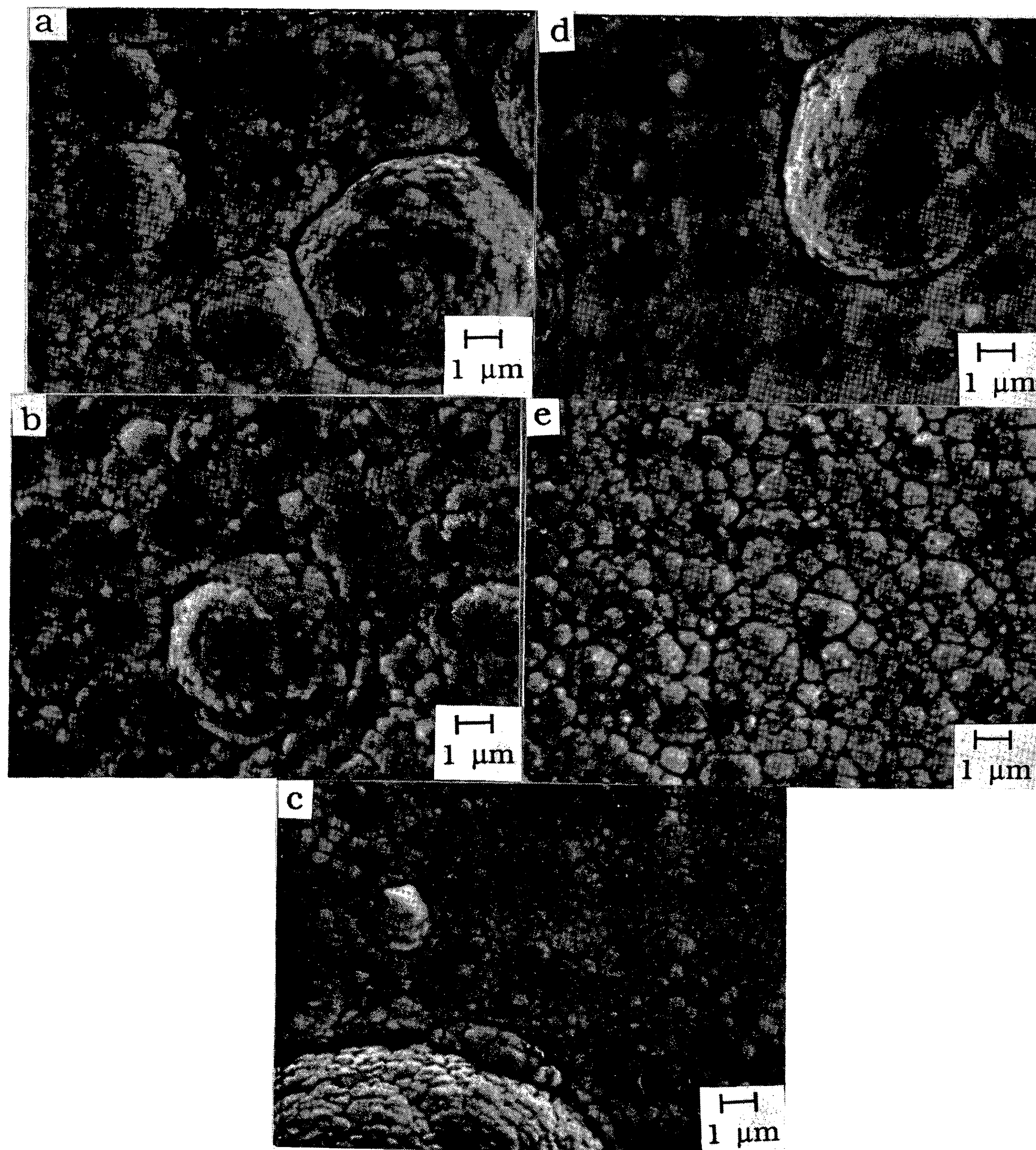

Figure 3.21: SEM photographs of surfaces of as-coated 13 ± 2-μm-thick sputtered silver coatings (5000X). The samples are arranged from the strongest {111} orientation to the strongest {220} orientation : a.) 0.55 amps b.) 0.20 amps c.) 0.40 amps (1st coating run) d.) 0.40 amps (2nd coating run) e.) 0.10 amps.

amperes. Two 0.40-ampere coating runs were again made at this thickness. The most common coating morphology was again a bimodal growth consisting of large domes surrounded by very fine grains. The coatings from the 0.20-ampere, the 0.30-ampere, the 0.45-ampere, the 0.50-ampere coating runs and the coating from the first 0.40-ampere coating all had this morphology. The 0.55-ampere coating had a similar morphology except the domes were much more closely packed and they were considerably smaller (1 to 5 μm in diameter). The surfaces of the 0.35-ampere coating sample and the second 0.40-ampere sample consisted of equiaxed grains with a few domed structures interspersed among them. The 0.40-ampere sample surface had a grain diameter of 2.45 μm and the 0.35-ampere sample surface had a grain diameter of 2.31 μm. Figure 3.22 shows SEM photographs of the 20-μm-thick coatings. The photographs are arranged from a strong {111} orientation to a strong {220} orientation. The coating morphologies were randomly distributed relative to the coating orientations and the bond strength was constant regardless of morphology.

SEM photographs of 0.40-ampere coatings in the thickness range of 1 μm to 43 μm are shown in Figure 3.23. For the very thin coatings (1 μm and 2 μm), there is very little development of a coating morphology. For these coating runs, the coatings still had the appearance of the machined copper substrate. The 6-μm-thick, 13-μm-thick and the 20-μm-thick coating have the typical bimodal

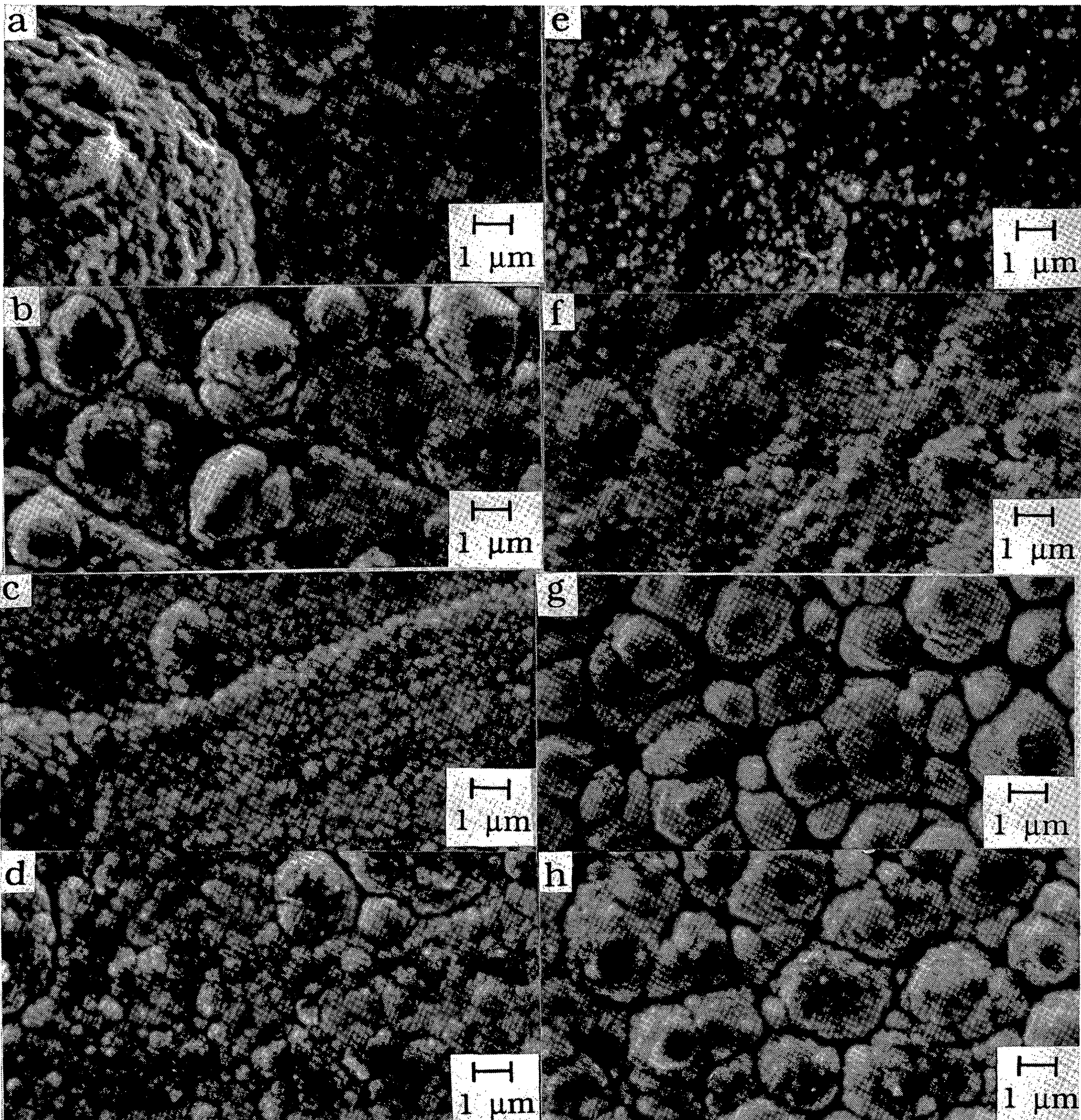

Figure 3.22: SEM photographs of surfaces of as-coated 20 ± 3-μm-thick sputtered silver coatings (5000X). The samples are arranged from the strongest {111} orientation to the strongest {220} orientation: a.) 0.45 amps b.) 0.55 amps c.) 0.50 amps d.) 0.30 amps e.) 0.20 amps f.) 0.40 amps (1st coating run) g.) 0.40 amps (2nd coating run) h.) 0.35 amps.

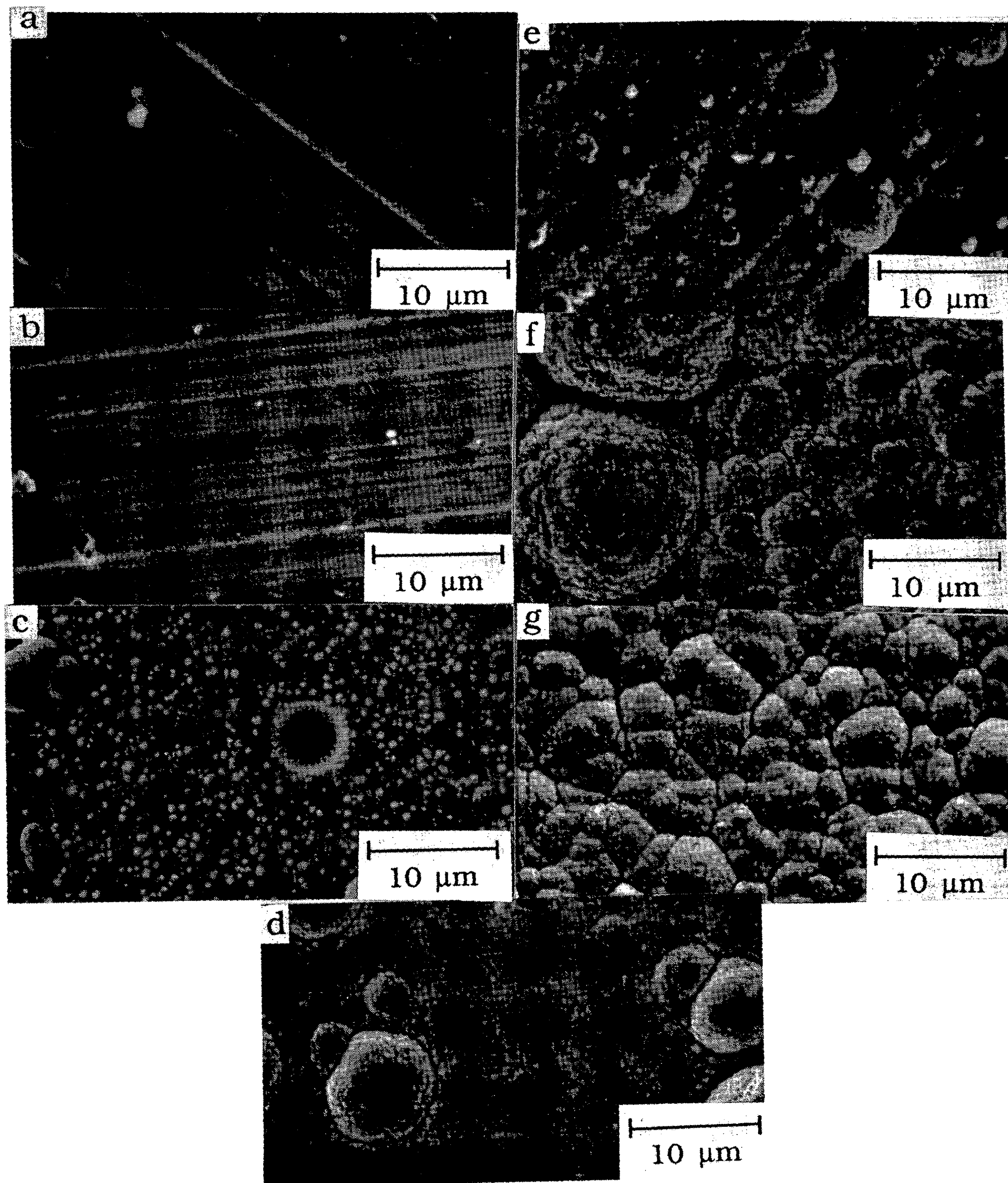

Figure 3.23: SEM photographs of the 0.40-amp coatings (2000X): a.) 1 μm b.) 2 μm c.) 6 μm d.) 13 μm e.) 20 μm f.) 35 μm g.) 43 μm.

growth structure with 1-μm-diameter to 10-μm-diameter domes. For the 35-μm-thick coating, there was still a bimodal domed structure but now the domes were much larger (usually 10 to 20 μm in diameter). Finally, for the thickest coating (43 μm), the structure was equiaxed grains with a diameter of 5.83 μm. This grain size is approximately 2.5 times larger than any of the grain sizes measured on the 20-μm-thick coatings. This suggests that a grain coarsening was taking place as the thickness increased. The increase in dome size with increasing thickness also substantiates this conclusion. Since thickness dominated all of the other parameters, no attempt was made to relate coating morphology to bond strength or orientation as a function of thickness.

C.3. Discussion of Coating Morphology Effects

In summary, a large variety of surface coating morphologies was observed. From one to three coating growth modes were observed on any one sample. The most common was a bimodal growth mode consisting of large domed structures (with a diameter of 1 to 10 μm), which were widely separated and surrounded by very fine grains. In all cases, the machining lines from the copper substrate could still be seen on the silver surface. There was no systematic change in morphology with changes in thickness or sputter deposition current. Even when two coating runs were done under the same conditions, the coating morphologies greatly varied.

An attempt was also made to correlate coating surface morphology with preferred orientation and bond strength. No correlation was found between coating morphology and either of these factors. Most of the coatings had a bimodal growth mode consisting of fine grains and large scattered domes. The exceptions were randomly distributed at different thicknesses, bond strengths and preferred orientations. Even the 20-μm-thick coatings had several very different surface morphologies while no change in bond strength was observed. Since the domes roughen the surface, they could have one of two effects. First, they could lower the bond strength by decreasing the initial contact area. A large amount of plastic deformation would be necessary to flatten the domes before contact could be made with the rest of the surface. They could also increase the bond strength by providing a more uniform distribution of initial contact sites which would lead to a more uniform contact area. More uniform contact would help to eliminate stress concentrations and bending moments when the joint was pulled in tension. Surprisingly, neither of these effects was observed. It may be because the dome heights were relatively small ($<< 0.25$ μm) compared to the height of the machining ridges, so that they did not affect the overall surface roughness. This could be checked with profilometry.

D. Fracture Surface Examination

Fracture surfaces were analyzed on several samples at each thickness. The analysis was complicated by the existence of several failure features on each fracture surface. At low magnifications (25X), all of the fracture surfaces had a very similar appearance. The machining lines from the two samples left a criss-crossed pattern (Figure 3.24). This pattern was not as distinct for the 20-μm-thick coatings as it was for the other thicknesses. For the thin coatings (1 μm and 2 μm), the crossed lines on the fracture surfaces were actually bonded regions which could be seen at 250X (Figure 3.25). All of the failure occurred within the silver and there was a relatively small contact area. All of the bonding occurred along the roughness peaks which produced a waffle pattern on the fracture surface. This supports the conclusion that the substrate surface roughness hinders the ability to make good contact in this thickness range. the bonded area fraction was measured for the thin coatings shown in Figure 3.25. The bonded area varied from 35 percent to 49 percent but it could not be related to bond strength:

Bond Strength (MPa)	Area Bonded (%)
8	43
129	35
179	49
222	47

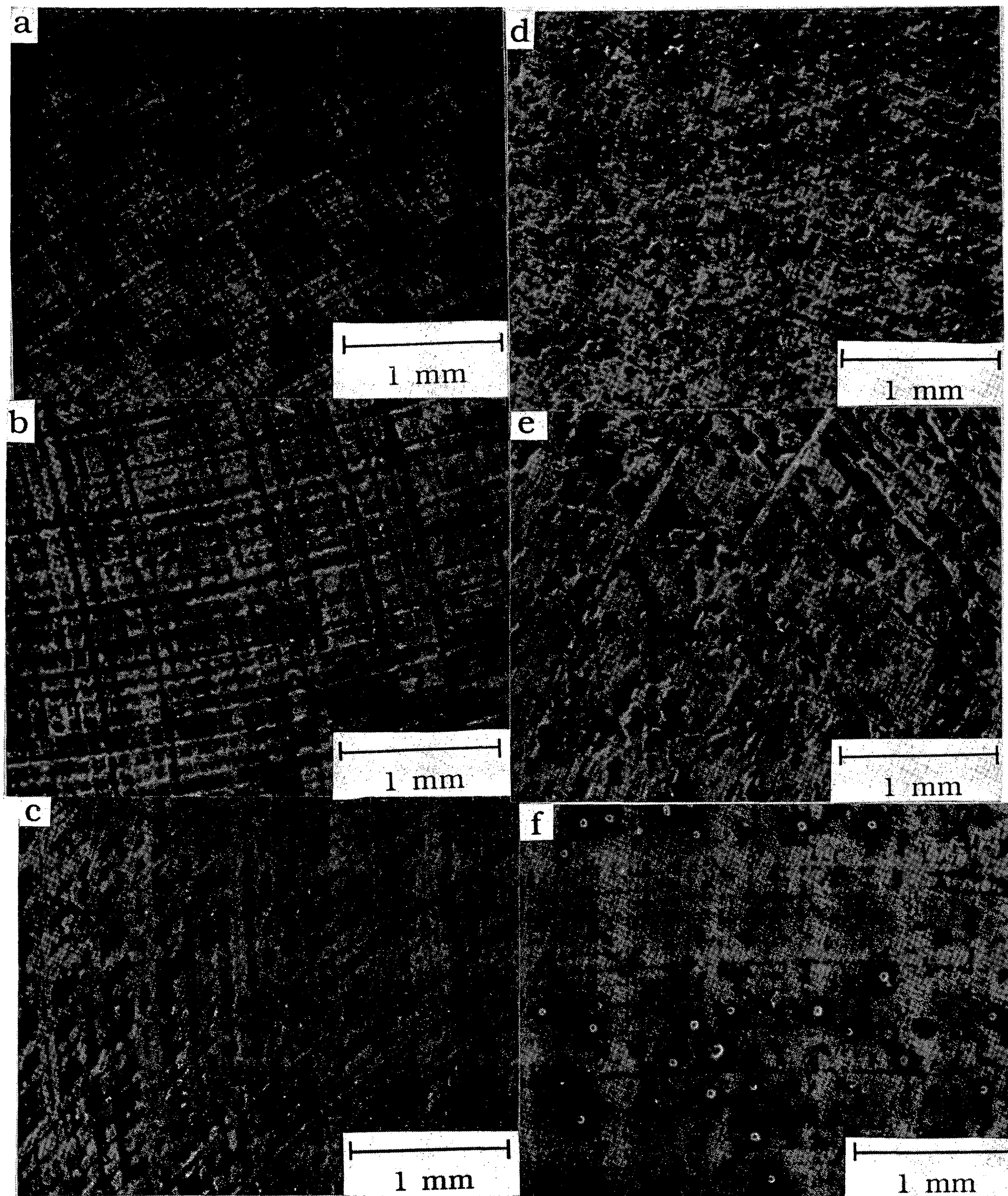

Figure 3.24: Low magnification (25X) photographs of fracture surfaces for several coating thicknesses: a.) 1 μm b.) 2 μm c.) 6 μm d.) 13 μm e.) 20 μm f.) 43 μm.

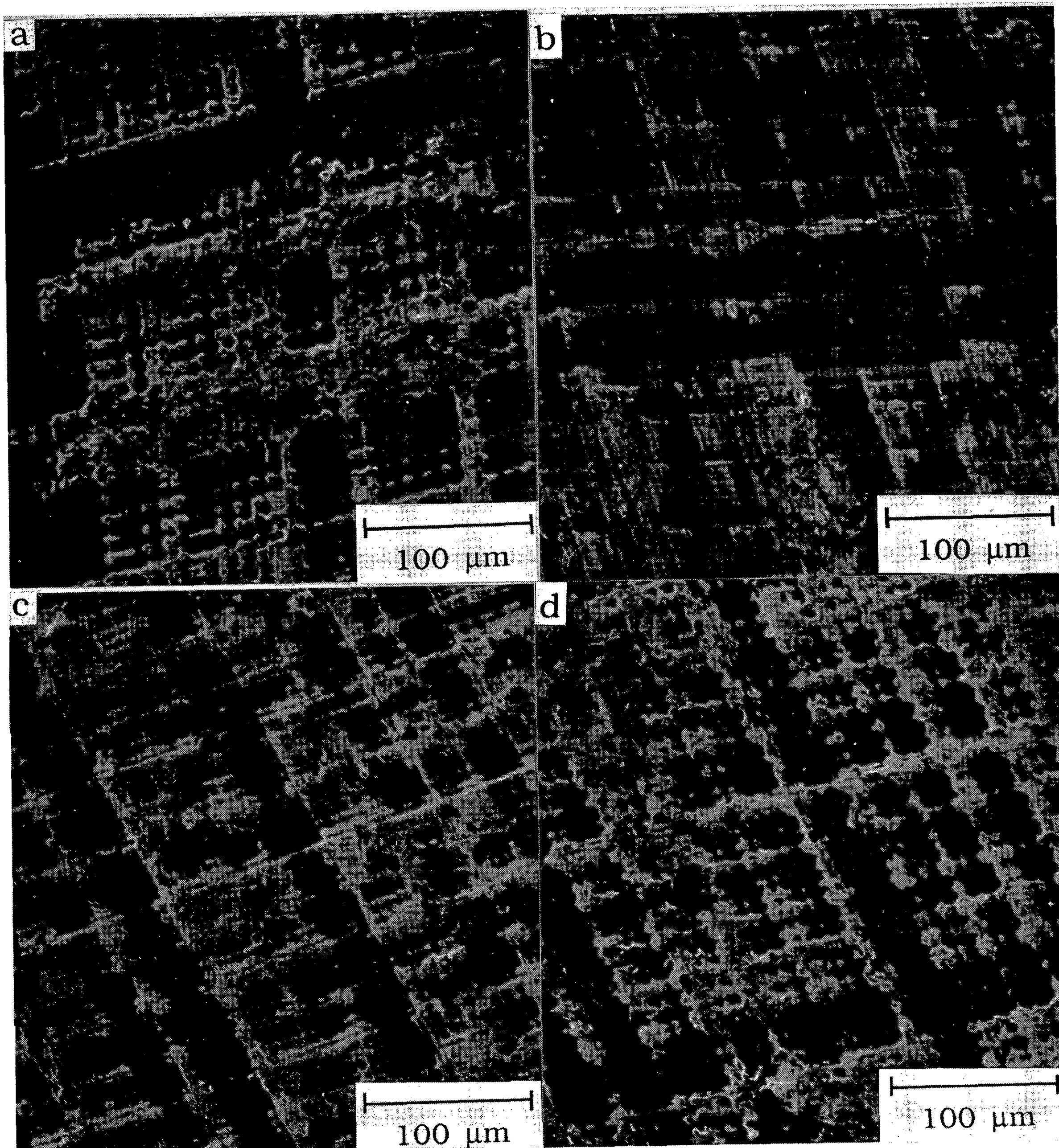

Figure 3.25: SEM photographs of fracture surfaces for thin coatings (250X): a.) 1 μm, bond strength = 8 MPa b.) 1 μm, bond strength = 129 MPa c.) 2 μm, bond strength = 179 MPa d.) 2 μm, bond strength = 226 MPa.

At 250X, the fracture surfaces of the 6-μm-thick to 35-μm-thick coatings were very different from the thinner coatings. All of these fracture surfaces were almost completely bonded. The criss-cross pattern on the surfaces was because of two different failure modes. The fracture surfaces had regions of both silver-silver failure and copper-silver deadhesion failure. The failure regions had a tendency to follow along the copper machining lines. Even for the same thickness and approximately the same bond strength, very different fracture patterns were observed (Figure 3.26).

Finally, the 43-μm-thick coating's fracture surface consisted of only silver-silver failure and its relative contact area had decreased to less than forty percent (Figure 3.27). As the thickness increased, a decrease in bond strength was expected since the constraints necessary for the development of a triaxial stress state in the joint are diminished in thicker coatings. This should not have led to a decrease in contact area. Instead, the contact area should have been approximately the same as for the 35-μm-thick coatings. It was the relative area fraction silver-silver failure region which should have increased as triaxiality was lost within the joint. The lack of contact suggested a decrease in deformation during bonding which was not expected.

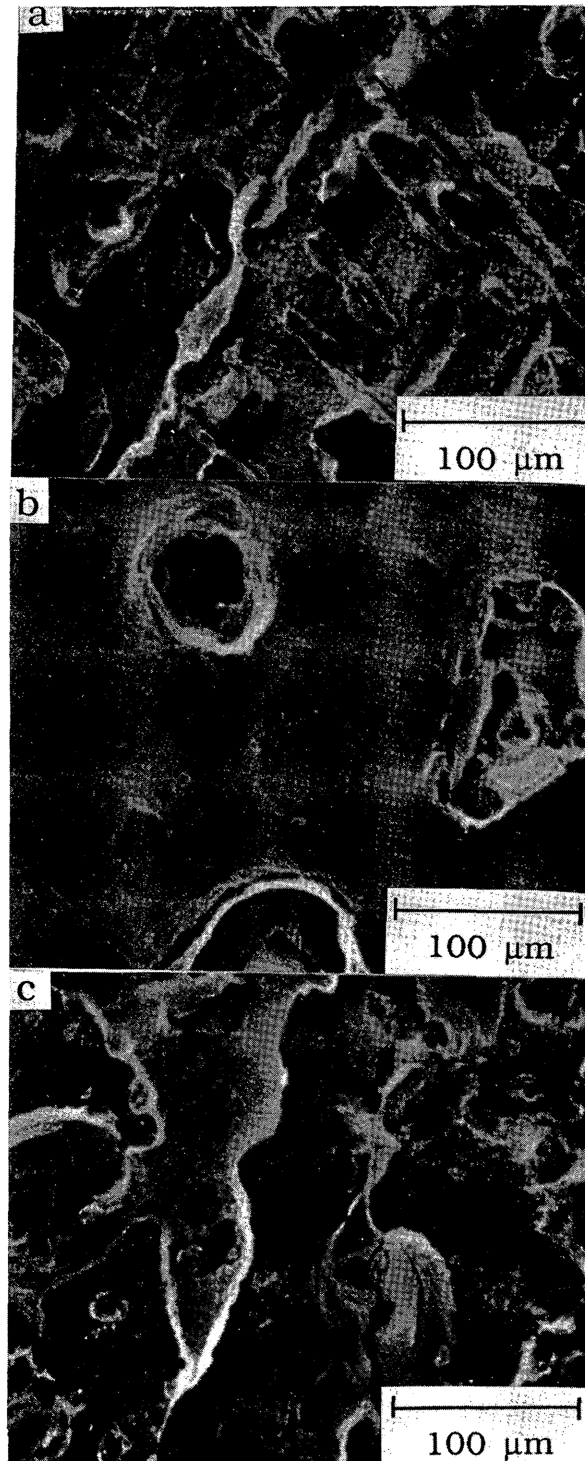

Figure 3.26: SEM photographs of fracture surfaces for 20-μm-thick coatings (250X): a.) bond strength = 233 MPa b.) bond strength = 243 MPa c.) bond strength = 243 MPa.

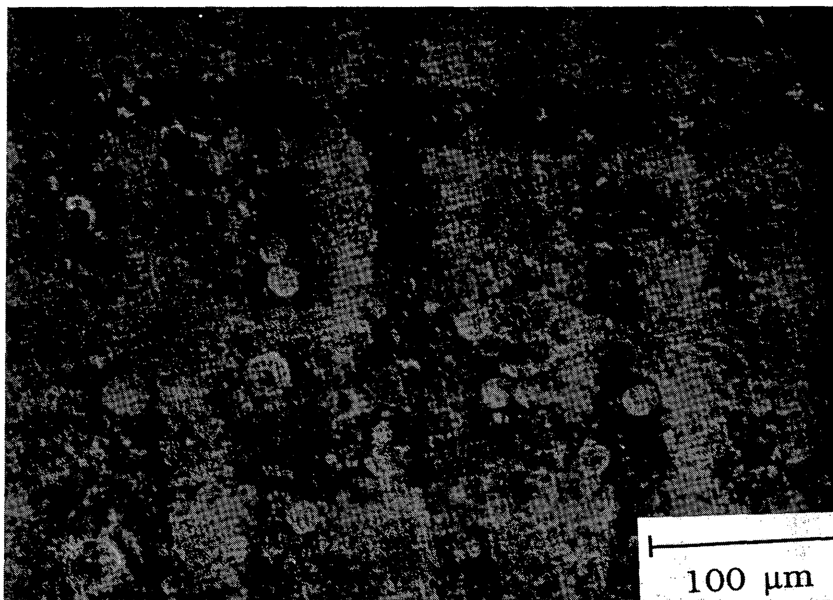

Figure 3.27: SEM photograph of the fracture surface of a 43-μm-thick coating (250X). The bond strength was 118 MPa.

IV. Conclusions

Sputter coated interlayers were used to solid state bond copper tensile halves. The results led to five conclusions:

1. Sputter coating represents a viable means of preparing interlayers for solid-state bonding. Full strength joints were achieved between ETP 110 copper samples using sputtered silver interlayers. At a joint thickness of 41 ± 6 μm, 11 out of 29 of the bonds tested failed in the copper substrate when joined for 30 minutes at 300 °C with a bonding pressure of 65 MPa (10 ksi). At this thickness all of the bond strengths were between 224 and 254 MPa. These strength values are all above the yield strength range of copper and several were in the ultimate strength range.

2. Thickness was found to be the dominant factor in determining bond strength. Three different regions of bond strength behavior were observed. From 2 μm to 35 μm, surface roughness effects caused a lowering of the average bond strength with decreasing thickness. In this region, a wide range of measured bond strengths were obtained at a given thickness. The range decreased with increasing thickness. In the second thickness region (35 μm to 70 μm), a triaxial stress state was developed within the joint. Very strong bonds were obtained and the measured bond strengths were all within a very narrow strength range. From 70 μm to 86 μm, thickness

effects led to a loss of the triaxial stress state within the joint. As the thickness increased, the bond strength decreased until it was slightly below the ultimate tensile strength of silver. The Orowan model for brazed joints was too simple to predict the bond strength for solid-state bonds. This is because the joints had a silver-silver bond line within the joint while the model assumes a uniform disc of material. Along this silver-silver interface, there can be voids and non-bonded regions. These imperfections in the joint made a triaxial stress state more difficult to maintain. The bond strength only varied with sputter deposition current for thin coatings (6 μm) and the relationship was not direct.

3. In the sputter deposition current range of 0.20 to 0.55 amperes, it was possible to predict whether a silver coating deposited on copper would have a {111} or a {220} preferred orientation at a given thickness. The degree of preferred orientation could not be predicted. Outside of this current range, it was not possible to predict the preferred orientation.

4. The bond strength was proportional to the degree of preferred orientation for a joint thickness of 12 μm. The strongest bonds were achieved with a highly preferred {220} orientation of the interlayer, while the weakest bonds occured with a strong {111} orientation. This may be due to easier plastic flow with a {220} interlayer

orientation leading to a higher contact area. For thicker coatings, the bond strength was constant regardless of orientation.

5. Most of the coatings exhibited a bimodal growth mode consisting of large domed structures (1 μm to 10 μm in diameter) surrounded by very fine grains (< 0.1 μm diameter). Some of the coatings exhibited other single modal, bimodal and trimodal growth modes. These different growth modes did not have any effect on the bond strength or preferred orientation.

V. References Cited

1. W. A. Owczarski and D. F. Paulonis, "Applications of Diffusion Welding in the USA," Welding Journal 22 (2), pp. 22-33 (1981).

2. B. Derby and E. R. Wallach, "Theoretical Model for Diffusion Bonding," Metal Science 16 (1), pp. 49-56 (1982).

3. B. Derby and E.R. Wallach, "Diffusion Bonding: Development of a Theoretical Model," Metal Science 18 (9), pp. 427-431 (1984).

4. H. A. Mohamed and J. Washburn, "Mechanism of Solid-State Pressure Welding," Welding Journal 54 (9), Research Supplement, pp. 302-s - 310-s (1975).

5. Kazakov, N.F. (Ed.), Diffusion Bonding of Materials, Pergamon Press Inc., New York, pp. 17-21 (1985).

6. C. L. Cline, "An Analytical and Experimental Study of Diffusion Bonding," Welding Journal 45 (11), Research Supplement, pp. 481-s - 489-s (1966).

7. H. J. Saxton, A. J. West and C. R. Barrett, "Deformation and Failure of Brazed Joints-Macroscopic Considerations," Metallurgical Transactions 2, pp. 999-1007 (1971).

8. Rosenquist,Terkel, Principles of Extractive Metallurgy, McGraw-Hill Book Company, New York, pp. 516-517 (1974).

9. Z. A. Munir, "A Theoretical Analysis of the Stability of Surface Oxides During Diffusion Welding of Metals," Welding Journal 62 (12), Research Supplement, pp. 333-s - 336-s (1983).

10. J. L. Knowles and T. H. Hazlett, "High-Strength Low-Temperature Bonding of Berylium and Other Metals," Welding Journal 49 (6), Research Supplement, pp. 301-s - 309-s.

11. J. W. Dini, W. K. Kelley, W. C. Cowden and E. M. Lopez, "Use of Electrodeposited Silver as an Aid in Diffusion Welding," Welding Journal 63 (1), Research Supplement, pp. 26-s - 34-s (1984).

12. I. M. Barta, "Low Temperature Diffusion Bonding of Aluminum Alloys," Welding Journal 43 (6), Research Supplement, pp. 243-s - 247-s (1964).

13. C. H. Crane, D. T. Lovell, W. A. Baginski and M. G. Olsen, "Diffusion Welding of Dissimilar Metals," Welding Journal 46 (1), Research Supplement, pp. 23-s - 31-s (1967).

14. P. S. McLeod and G. Mah, "The Effects of Substrate Bias Voltage on the Bonding of Evaporated Silver Coatings," Journal of Vacuum Science Technology 11 (1), pp. 119-121 (1974).

15. E. R. Naimon, D. Vigil, J. P. Villegas and L. Williams, "Adhesion Study of Silver Films Deposited from a Hot Hollow-Cathode Source," Journal of Vacuum Science Technology 13 (6), pp. 1131-1134 (1976).

16. E. R. Naimon, J. H. Doyle, C. R. Rice, D. Vigil and D. R. Walmsley, "Diffusion Welding of Aluminum to Stainless Steel," Welding Journal 60 (11), pp. 17-20 (1981).

17. P. D. Calderon, D. R. Walmsley and Z. A. Munir, "An Investigation on the Diffusion Welding of Pure and Alloyed Aluminum to Type 316 Stainless Steel," Welding Journal 64 (4), Research Supplement, pp. 104-s - 112-s (1985).

18. Carl Schalansky, Z. A. Munir and D. L. Walmsley, "An Investigation on the Bonding of Hot Hollow-Cathode Deposited Silver Interlayers to Type 304 Stainless Steel," Journal of Materials Science 22, pp. 745-751 (1987).

19. K. L. Chopra, Thin Film Phenoma, McGraw-Hill Book Company, New York, Chapters II and IV (1970).

20. W. D. Westwood, "Sputter Deposition Processes," MRS Bulletin 13 (12), pp. 46-51 (1988).

21. Chapman, Brian N. and Anderson, J. C. (Eds.), Science and Technology of Surface Coating, Academic Press, New York, pp. 369-384 (1974).

22. H. F. Winters, R. P. H. Chang, C. J. Mogab, J. Evans, J. Thornton and H. Yasuda, "Coatings and Surface Modification Using Low Pressure Non-equilibrium Plasmas," Materials Science and Engineering 70 pp. 53-77 (1985).

23. T. G. Nieh and J. Wadsworth, "Thick Magnesium Films Produced by Deposition Techniques," Thin Solid Films 152, pp. 525-534 (1987).

24. Hyung J. Lee, "Texture and Morphology of Sputtered Cr Thin Films," Journal of Applied Physics 57 (1), pp. 4037-4039 (1985).

25. A. F. Jankowski and T. O. Wilford. "Grain Size Variations in Coatings," Journal of Metals (6), pp. 28-30 (1987).

26. Norman H. Nicholas, "Influence of Surface Topography on Low Temperature Solid State Bonding," Masters Thesis T-3643, Colorado School of Mines (1990).

27. Roger A. Nichting, "An Investigation of Time-Temperature Dependent Deformation Behavior in Low Temperature Solid State Bonding of Copper," Ph. D. Dissertation T-3697, Colorado School of Mines (1989).

28. Nikolajs Bredz, "Investigation of Factors Determining the Tensile Strength of Brazed Joints," Welding Journal 33 (11), Research Supplement, pp. 545-s - 563-s (1954).

29. N. Bredz and H. Schwartzbart, "Triaxial Tension Testing and the Brittle Strength of Metals," Welding Journal 35 (12), Research Supplement, pp. 610-s - 615-s (1956).

30. M. O'Brien, C. R. Rice and D. L. Olson, "High Strength Diffusion Welding of Silver Coated Base Metals," Welding Journal 55 (1), Research Supplement, pp. 25-27 (1976).

31. Reed-Hill, Robert E., Physical Metallurgy Principles, PWS Publishers, Boston, p. 178 (1973).